Available online at www.sciencedirect.com
SCIENCE DIRECT®
Journal of Computational Physics 213 (2006) 777–802
JOURNAL OF COMPUTATIONAL PHYSICS
www.elsevier.com/locate/jcp

Optimization of time integration schemes coupled to spatial discretization for use in CAA applications

Jan Ramboer *, Tim Broeckhoven, Sergey Smirnov, Chris Lacor

Department of Fluid Mechanics, Vrije Universiteit Brussel, Pleinlaan 2, 1050 Brussel, Belgium

Received 21 February 2005; received in revised form 12 August 2005; accepted 15 August 2005
Available online 10 October 2005

Abstract

In this paper errors arising from spatial and temporal discretization are discussed. A new formulation to optimize time integration schemes is proposed. The new optimization also takes the errors coming from the spatial discretization into account, which leads to a minimization of the total errors. It is applicable to central and upwind type spatial discretizations. A six stage Runge–Kutta scheme is optimized for central and upwind spatial discretizations. Its efficiency is demonstrated on a one dimensional convection equation and on a Linearized Euler problem. The results indicate an important improvement.

Keywords: Computational aero acoustics; Time integration; Optimization

1. Introduction

In the field of computational aero acoustics (CAA) one is interested in the prediction of sound far from its source. Several characteristics of the acoustic waves require that special attention is paid to the spatial and temporal discretization schemes. First of all, acoustic waves are non-dispersive and non-dissipative in their propagation and therefore can travel over long distances in all directions. Secondly, the amplitudes of acoustic waves are several orders of magnitude smaller than normal aerodynamic perturbations. These characteristics put more stringent requirements on the numerical schemes used in CAA.

The last few years, much attention has been paid to the use of spatial discretizations in CAA. The accuracy of the spatial discretization schemes needed in CAA is higher than those of classical CFD codes, where usually a second order discretization is sufficient. However, taking into account the acoustic properties of the sound waves in CAA, the actual order or the scheme is of less importance than its dispersive and dissipative behavior. This information, which is related to the resolution of the scheme (as opposed to the accuracy) can be obtained from a Fourier mode analysis [1]. The resolution is then the ability of the scheme to accurately represent Fourier modes of increasing wave number. The dispersion errors of the scheme cause an error in the phase of the

* Corresponding author. Tel.: +32479947422; fax: +3226292880.
E-mail address: jan@stro.vub.ac.be (J. Ramboer).

0021-9991/$ - see front matter
doi:10.1016/j.jcp.2005.08.033

Fourier waves, as compared to the exact solution from the differential equation, whereas the dissipation errors cause an error in the amplitude of the Fourier waves. In CAA compact or Padé type schemes are often used in a Finite Difference formulation [2,3]. Recently, Finite Volume formulations were developed, e.g. [4,5], which are directly applicable on arbitrary structured meshes and [6] where a Jacobian transformation to Cartesian grids has to be used.

Similar arguments apply to the temporal discretization. The acoustic waves have to be tracked accurately in time. Time integration schemes can be optimized for different properties, such as linear and non linear stability, accuracy efficiency, error control reliability and dissipation and dispersion accuracy [7]. When one is especially concerned about the dissipative and dispersive behavior of discretized equations, optimization of dissipation and dispersion properties of the time integration scheme is of paramount importance. By far the most popular schemes in CAA are the Runge–Kutta schemes. They are explicit and can be formulated up to an arbitrary order of accuracy. Many authors use the classical Runge–Kutta schemes, whether or not in a low storage form to reduce memory usage. Until now not many authors have considered optimizing time integration schemes. A few articles mention optimized Runge–Kutta schemes with better dissipative and dispersive behavior.

A commonly used optimized time integration scheme is the one by Hu et al. [8]. Several Runge–Kutta schemes are optimized for their dispersive and dissipative behavior and are baptized as low-dissipation and low-dispersion Runge–Kutta schemes (LDDRK). Hu et al. give the coefficients in [8] for a four, five and a six stage optimized Runge–Kutta scheme. All of these are kept second order accurate in time while minimizing the dispersion and dissipation errors. A second method used by Hu et al. [8] to optimize time integration schemes is to use different coefficients for the Runge–Kutta schemes in two alternating time steps. This leads to a further reduction of the dispersion and dissipation errors while maintaining a higher order of accuracy. Two fourth order optimized schemes are described in [8], a 4–6 alternating scheme and a 5–6 alternating scheme.

In his extensive study on different numerical methods used in CAA Goodrich [9] concludes that the six stage optimized low dissipation and dispersion Runge–Kutta scheme by Hu [8] in combination with at least a sixth order spatial differencing can provide between one and two orders of magnitude decrease in error at a given grid density. However the fourth order central and the DRP spatial differencing by Tam et al. [10] do not obtain an advantage of the optimized scheme. Ewert et al. [11] use the fourth order alternating two step low dissipation and dispersion Runge–Kutta scheme (LDDRK 5–6) formulated by Hu [8] in combination with the fourth order spatial DRP scheme of Tam et al. [10] in their two step CFD/CAA approach. In the ALESIA code used by Bogey et al. [12,13] the four stage optimized scheme, described in [8], is applied. Also Morris et al. [14] use the four stage optimized Runge–Kutta scheme to integrate the Non Linear Perturbation equations in time. Recently, Bogey et al. present an optimization of Runge–Kutta schemes based on similar ideas as in Hu et al. The integrals to be optimized are defined somewhat differently leading to different schemes [15]. Another recent proposed optimized scheme is the one by Calvo et al. [16]. The scheme is a 2N-storage six-stage Runge–Kutta scheme. It was optimized both for its dissipative and dispersive properties, as well as for its stability. Tam et al. [10] are one of the few authors who optimized a four level time integration scheme. The procedure is comparable to the one followed by Hu et al. [8].

In this paper, a new way of optimizing the temporal integration schemes is presented. The optimization processes found in the literature so far, took only the dissipation and dispersion errors introduced by the temporal discretization into account. However the performance of a code will depend on the total dispersion and dissipation errors introduced by spatial and temporal discretization. By taking into account the spatial discretization during the optimization process of the temporal scheme, the total dissipation and dispersion error can be minimized instead of only the temporal error. Because the optimization of the time integration scheme is coupled to the spatial discretization, it can also be applied to upwind type schemes, as opposed to optimization procedures along the imaginary axis.

The outline of the paper is as follows. Section 2 gives a short introduction in the Fourier analysis of the errors introduced by the spatial and temporal discretization. Next, in Section 3 the common optimization process and the newly proposed optimization process are explained. Further on, in Section 4, the results are shown for a series of test problems. The main conclusions are given in the final section.

2. Dispersion and dissipation errors

Consider the scalar convection equation

$$\frac{\partial u}{\partial t} + a\frac{\partial u}{\partial x} = 0 \tag{1}$$

and a Fourier wave

$$\hat{u} = F(t)\mathrm{e}^{Ikx}. \tag{2}$$

Substitution of (2) in (1) gives the following equation for F:

$$\frac{\mathrm{d}F}{F} = -Iak\,\mathrm{d}t. \tag{3}$$

Solution of this equation gives

$$F = \mathrm{e}^{-Iakt} \tag{4}$$

and the Fourier wave of type (2) satisfying Eq. (1) exactly is given by

$$\hat{u}_{\mathrm{ex}} = \mathrm{e}^{Ik(x-at)}. \tag{5}$$

2.1. Dispersion and dissipation errors of the spatial scheme

We consider again Eq. (1), but semi-discretized in the sense that a spatial discretization scheme is used for the spatial derivative. Eq. (1), written in point i becomes:

$$\frac{\partial u_i}{\partial t} = R(u_i, u_{i-1}, u_{i+1}, u_{i-2}, u_{i+2}, \ldots) \tag{6}$$

with R the discretization stencil of $-a\frac{\partial u_i}{\partial x}$. The letter R is used to indicate that this is the so-called residual. Depending on the scheme used, the value of u in point i, u_i, as well as in surrounding cells (u_{i-1}, u_{i+1}, $u_{i-2}, u_{i+2}, \ldots$) may be used.

Substitution of the Fourier wave (2) leads to the following equation for F:

$$\frac{\mathrm{d}F}{F} = \mathscr{R}\,\mathrm{d}t, \tag{7}$$

where $\mathscr{R}$ is the so-called Fourier footprint of the residual, which can be decomposed in a real part, $\mathscr{R}_{\mathrm{r}}$, and an imaginary part, $\mathscr{R}_{\mathrm{i}}$:

$$\mathscr{R} = \mathscr{R}_{\mathrm{r}} + I\mathscr{R}_{\mathrm{i}}. \tag{8}$$

The solution of (7) is

$$F = \mathrm{e}^{\mathscr{R}_{\mathrm{r}}t}\mathrm{e}^{I\mathscr{R}_{\mathrm{i}}t}. \tag{9}$$

Combining Eqs. (2) and (9), the solution of the semi-discretized equation is therefore

$$\hat{u} = \mathrm{e}^{\mathscr{R}_{\mathrm{r}}t}\mathrm{e}^{Ik(x+\frac{\mathscr{R}_{\mathrm{i}}}{k}t)}. \tag{10}$$

Comparing Eq. (5) with (10) it can be observed that because of the discretization, two errors arise:

$$|r_{\mathrm{space}}|\mathrm{e}^{-I\delta_{\mathrm{space}}} = \frac{\mathrm{e}^{\mathscr{R}_{\mathrm{r}}t}\mathrm{e}^{Ik(x+\frac{\mathscr{R}_{\mathrm{i}}}{k}t)}}{\mathrm{e}^{Ik(x-at)}}. \tag{11}$$

- An error on the amplitude of the wave: the exact amplitude is 1 whereas, with spatial discretization, an amplitude $|r_{\mathrm{space}}| = \mathrm{e}^{\mathscr{R}_{\mathrm{r}}t}$ is obtained. This is the dissipation error.

- An error on the propagation speed of the wave: the exact speed is 'a' (for all wave numbers 'k') whereas, with spatial discretization, the wave speed depends on the wave number and is given by $\delta_{\text{space}} = -\frac{\mathscr{R}_i}{k}$. This is the dispersion error.

  Some authors define a numerical wave number k^* as

$$\mathscr{R} \equiv -Iak^*. \tag{12}$$

The solution of the semi-discretized Eq. (9) becomes:

$$\hat{u} = \mathrm{e}^{Ik(x-\frac{k^*}{k}at)}. \tag{13}$$

The difference between numerical and actual wave speed describes the error. The real part of k^* corresponds to dispersion errors, whereas the imaginary part corresponds to a dissipation error.

As an example, consider the second order central scheme:

$$\frac{\partial u_i}{\partial t} + a\frac{u_{i+1} - u_{i-1}}{2\Delta x} = 0. \tag{14}$$

The Fourier footprint is given by:

$$\mathscr{R} = -Ia\frac{\sin(k\Delta x)}{\Delta x}. \tag{15}$$

The Fourier footprint is purely imaginary and hence the central scheme does not introduce a dissipation error. The dispersion error, Φ_{disp}, defined as the ratio of numerical wave speed and exact wave speed, is given by:

$$\Phi_{\text{disp}} = \frac{\sin(k\Delta x)}{k\Delta x}. \tag{16}$$

2.2. Dispersion and dissipation errors of temporal scheme

We consider the semi-discretized Eq. (6) and introduce a temporal discretization. To fix thoughts, consider the Euler explicit scheme:

$$\frac{u_i^{n+1} - u_i^n}{\Delta t} = R(u_i^n, u_{i-1}^n, u_{i+1}^n, u_{i-2}^n, u_{i+2}^n, \ldots), \tag{17}$$

where the superscript indicates the time level of the solution. Substitution of the Fourier wave (2) gives

$$\frac{F^{n+1} - F^n}{\Delta t} = \mathscr{R}F^n \tag{18}$$

and

$$\frac{F^{n+1}}{F^n} = 1 + \Delta t\mathscr{R}. \tag{19}$$

To study the stability of the temporal discretization it suffices to check that $|\frac{F^{n+1}}{F^n}| \leqslant 1$. For a study of dispersion and dissipation properties, the correct evolution of F in time has to be considered. This is given by Eq. (9) and hence

$$\left(\frac{F^{n+1}}{F^n}\right)_{\text{ex}} = \mathrm{e}^{\mathscr{R}\Delta t}. \tag{20}$$

Comparison of Eqs. (19) and (20) shows that, for a given spatial discretization scheme, the temporal discretization in general introduces both an error in the module of F (the dissipation error) and in the phase of F (the dispersion error).

This analysis is easily extendable to other discretization schemes, e.g., for explicit Runge–Kutta schemes Eq. (19) becomes:

$$\frac{F^{n+1}}{F^n} = G(\mathscr{R}\Delta t), \tag{21}$$

where G is a polynomial of degree q, with q the number of Runge–Kutta stages. This polynomial is an approximation of the exponential function $e^{\mathscr{R}\Delta t}$.

The numerical error introduced by the temporal discretization is given by comparing $G(\mathscr{R}\Delta t)$ with $e^{\mathscr{R}\Delta t}$:

$$\frac{G(\mathscr{R}\Delta t)}{e^{\mathscr{R}\Delta t}} = |r|e^{-I\delta}, \tag{22}$$

where $|r|$ is the dissipation error introduced by the temporal discretization and δ the dispersion error.

Fig. 1 shows the temporal dissipation and dispersion error for a standard 4 stage Runge–Kutta scheme (RK4) with a fourth order Finite Volume Compact Scheme for the spatial discretization [5] at a CFL number of 1.5. The figure shows the residual footprint ($\mathscr{R}$) of the spatial discretization, the stability limit of the discretization ($|G(\mathscr{R}\Delta t)| = 1$) and the contour lines of the temporal dissipation and dispersion error.

By plotting the temporal error, given in Fig. 1, along the imaginary axis, the dissipation and dispersion error are found in function of the wave number (for central schemes only). These one dimensional plots are often used in other articles such as that of Hu et al. [8]. The plots of Fig. 1 however also give some insight in the error behavior of the upwind schemes. A time integration scheme with low dissipation and dispersion errors is found when the Fourier footprint of the spatial discretization is in the regions of isolines $|r| = 1$ in the left plot and in the region of $\delta = 0$ in the right plot.

2.3. Dispersion and dissipation errors of total scheme

The total dissipation and dispersion error introduced by discretizing Eq. (1) in time and space, is obtained by comparing $G(\mathscr{R}\Delta t)$ with $e^{-Iak\Delta t}$. From Eq. (23) it is easily seen that the total dissipation error is the product of the spatial dissipation error with the temporal dissipation error, while the total dispersion error is the sum of both

$$\frac{G(\mathscr{R}\Delta t)}{e^{-Iak\Delta t}} = \frac{G(\mathscr{R}\Delta t)}{e^{\mathscr{R}\Delta t}}\frac{e^{\mathscr{R}\Delta t}}{e^{-Iak\Delta t}} = (|r_{\text{space}}||r_{\text{time}}|)e^{-I(\delta_{\text{space}}+\delta_{\text{time}})} = |r_{\text{total}}|e^{-I\delta_{\text{total}}}. \tag{23}$$

Fig. 2 shows the total dissipation and dispersion errors plotted as a function of $k\Delta x$ for a standard 4 stage Runge–Kutta scheme (RK4) with a fourth order Finite Volume Central Compact Scheme for the spatial discretization [5] at a CFL number of 1.5.

Since the spatial discretization is done with a central scheme, only the time discretization is responsible for the dissipation error.

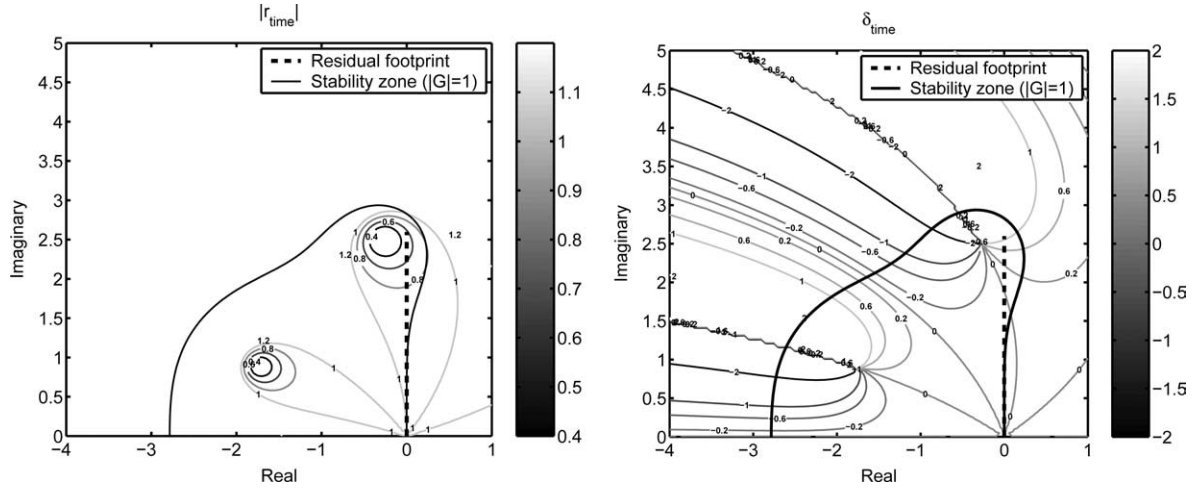

Fig. 1. $|r|$ (left) and δ (right) for the temporal discretization with a RK4 scheme, CFL = 1.5.

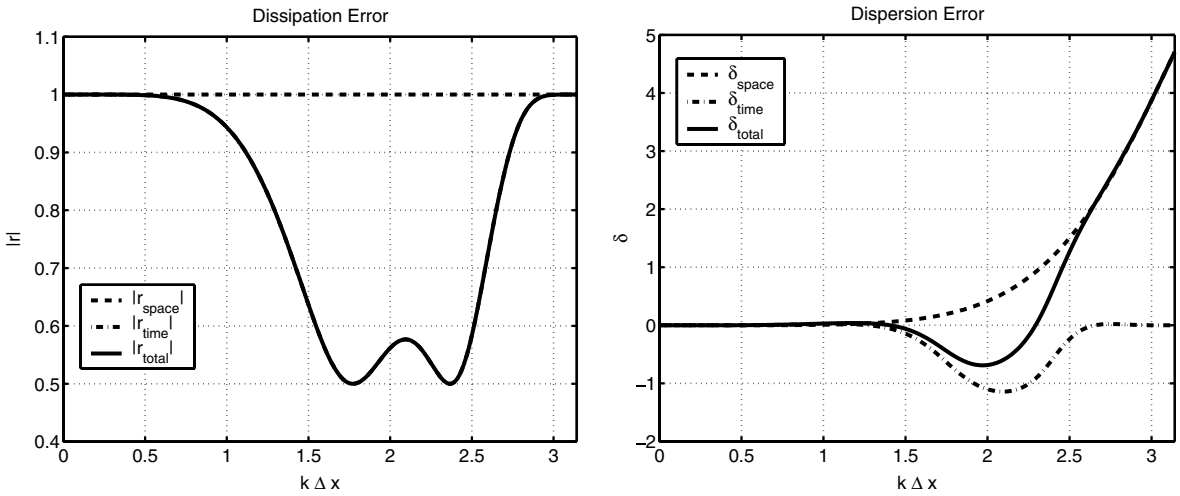

Fig. 2. Dissipation and dispersion errors, CFL = 1.5.

3. Optimization

In the present paper, the optimization of time advancing schemes, in particular the Runge–Kutta schemes, is considered. The following initial value problem is considered:

$$\frac{\mathrm{d}\mathbf{U}}{\mathrm{d}t} = \mathbf{F}(t, \mathbf{U}(t))\mathbf{U}(t=0) = \mathbf{U}_0 \tag{24}$$

with $\mathbf{U}$ the vector of unknowns. The most general q-stage explicit Runge–Kutta scheme [7], to integrate from time level t^n to time level t^{n+1}, can be written as:

$$\mathbf{U}^{(i)} = \mathbf{U}^{(n)} + \Delta t \sum_{j=1}^{i-1} a_{ij}\mathbf{F}^{(j)}, \tag{25}$$

$$\mathbf{U}^{(n+1)} = \mathbf{U}^{(n)} + \Delta t \sum_{j=1}^{q} b_j\mathbf{F}^{(j)}, \tag{26}$$

where

$$\mathbf{F}^{(i)} = \mathbf{F}(t^{(i)}, \mathbf{U}^{(i)}), \tag{27}$$

$$t^{(i)} = t^{(n)} + c_i\Delta t, \tag{28}$$

$$c_i = \sum_{j=1}^{s} a_{ij} \tag{29}$$

and the stage number i runs from 1 to q. The above formulation requires a lot of memory because at stage i all $\mathbf{F}^{(j)}$ on the previous stages need to be known. The Runge–Kutta schemes can be implemented in a form which requires less storage, given by:

$$\mathbf{U}^{(i)} = \mathbf{U}^{(n)} + \Delta t\alpha_i\mathbf{F}^{(i-1)}, \tag{30}$$

$$\mathbf{U}^{(n+1)} = \mathbf{U}^{(n)} + \Delta t \sum_{i=1}^{q} \beta_i\mathbf{F}^{(i)}. \tag{31}$$

A classical Runge–Kutta scheme used in CFD applications is:

$$\mathbf{U}^{(i)} = \mathbf{U}^{(n)} + \Delta t\alpha_i\mathbf{F}^{(i-1)}, \tag{32}$$

$$\mathbf{U}^{(n+1)} = \mathbf{U}^{(n)} + \Delta t\mathbf{F}^{(q)}. \tag{33}$$

If $q = 4$ this scheme is fourth order accurate in time for linear advection problems with constant speed. In case of non linearity this scheme has a maximum accuracy in time of second order. The amplification factor of the Runge–Kutta scheme given by Eq. (32) is given by

$$G = 1 + \sum_{j=1}^{q} a_j (\mathscr{R}\Delta t)^j. \tag{34}$$

Here the coefficients a_j relate to α_i ($\alpha_1 = 0$) by

$$\begin{aligned} a_2 &= \alpha_q, \\ a_3 &= \alpha_q \alpha_{q-1}, \\ &\dots \\ a_q &= \alpha_q \alpha_{q-1} \dots \alpha_2. \end{aligned} \tag{35}$$

In CAA applications, where one is especially concerned about the dissipative and dispersive behavior of discretized equations, optimization of dissipation and dispersion properties of the time integration scheme is of paramount importance.

A very commonly used optimized time integration scheme is the one by Hu et al. [8]. Several Runge–Kutta schemes are optimized for their dispersion and dissipation behavior and are baptized as low-dissipation and low-dispersion Runge–Kutta schemes (LDDRK). The optimization is achieved by minimizing the difference between the numerical amplification factor, $G(\mathscr{R}\Delta t)$, and the exact temporal amplification factor, $e^{\mathscr{R}\Delta t}$, as explained in Section 2.2.

The following integral is therefore minimized:

$$\int_0^{\Gamma} |G(-I\sigma) - e^{-I\sigma}|^2 \, d\sigma \tag{36}$$

with $\sigma = I\mathscr{R}\Delta t$ and Γ specifies the range of σ in the optimization. However Hu et al. do not give an indication which value Γ is given during the optimization. It can be shown that the integral minimizes the sum of the dissipation and dispersion errors [8]. The coefficients are given in [8] for a four, five and a six stage optimized Runge–Kutta scheme (LDDRK4, LDDRK5, LDDRK6). All of these are kept fourth order accurate in time while minimizing the dispersion and dissipation errors.

This optimization implicitly supposes that one deals with a central spatial discretization because one integrates over σ, thus assuming σ is a real number. Looking in the complex plane, the optimization will only be valid on the imaginary axis. Upwind type spatial discretizations have however complex modified wave numbers k^*.

Also, Hu et al. minimize only the temporal errors by minimizing the difference between numerical amplification factor, $G(\mathscr{R}\Delta t)$, and the exact temporal amplification factor, $e^{\mathscr{R}\Delta t}$. The maximum allowable CFL number is then calculated by imposing an accuracy limit. For the fourth order Finite Volume Compact Central scheme [5] the maximum allowable CFL number according to Hu is 0.837. Fig. 3 shows the standard six stage Runge–Kutta scheme used with a fourth order Finite Volume Compact Central scheme [5]. Looking at the total dissipation error, it is immediately seen that the scheme is unstable because the error is bigger than one for a certain wave number range. The optimized six stage Runge–Kutta scheme by Hu is shown in Fig. 4. It is noticed that the scheme is stable and that the dissipation error is minimized. Compared to the total dispersion error of the standard six stage Runge–Kutta scheme, little improvement is found as the largest contribution to the total dispersion error comes from the spatial dispersion errors, which are not optimized.

In the recent paper of Calvo et al. [16], a 2N-storage six-stage Runge–Kutta scheme is developed to maximize the stability as well as to optimize its dissipative and dispersive properties. The optimization is done by maximizing the continuous function $\frac{1}{2}S + \frac{1}{2}L$, where S is the border of the stability zone:

$$S = \max\{\delta \geqslant 0; |G(Iv)| \leqslant 1 \quad \forall v \in [0, \delta]\} \tag{37}$$

and L is a measure associated to both dispersion $\phi(v) = v - \arg(G)$ and dissipation $d(v) = 1 - |G|$:

$$L = \max\{\lambda \geqslant 0; |d(v)| \leqslant |\phi(v)| \leqslant 1.25 \times 10^{-3} \quad \forall v \in [0, \lambda]\} \tag{38}$$

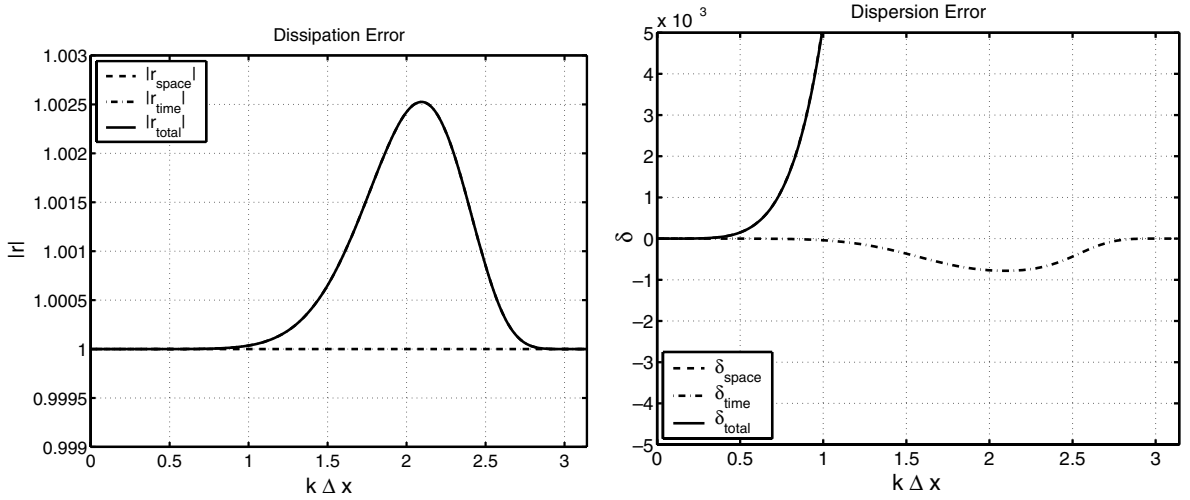

Fig. 3. Dissipation and dispersion errors standard RK6, CFL = 0.837.

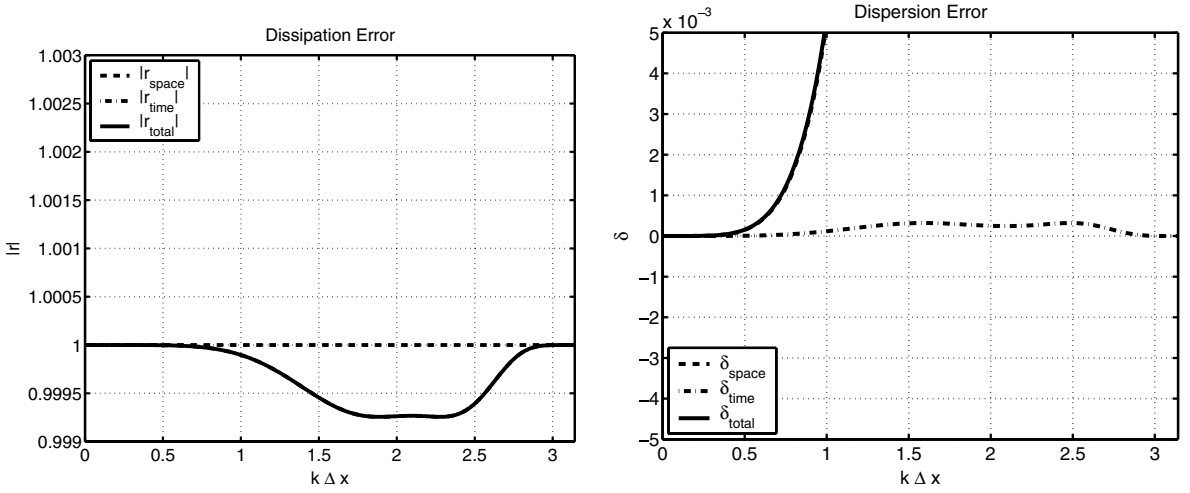

Fig. 4. Dissipation and dispersion errors Hu optimized RK6, CFL = 0.837.

with $v = -I\mathscr{R}\Delta t$. From Eq. (38) it is noted that also for this optimization only the temporal errors and not the total errors are minimized. This is illustrated in Fig. 5 which shows the dissipation and dispersion errors of the scheme proposed by Calvo et al. [16]. Since v is assumed to be a real number, also here the optimization is done along the imaginary axis and is thus only valid for central schemes (see Fig. 5).

In this paper, it is proposed to minimize the total dissipation and the total dispersion error for an arbitrary scheme (central or upwind) by plugging the residual footprint in the integral and minimizing the difference between numerical amplification factor, $G(\mathscr{R}(k\Delta x)\Delta t)$, and the exact amplification factor, $e^{-Iak\Delta t}$.

The following integral is therefore minimized:

$$\int_0^{\Gamma} |G(\mathscr{R}(k\Delta x)\Delta t) - e^{-Iak\Delta t}|^2 d(k\Delta x) \tag{39}$$

with the constraint for stability

$$|G(\mathscr{R}(k\Delta x)\Delta t)| < 1 \quad \forall k\Delta x \in [0, \pi] \tag{40}$$

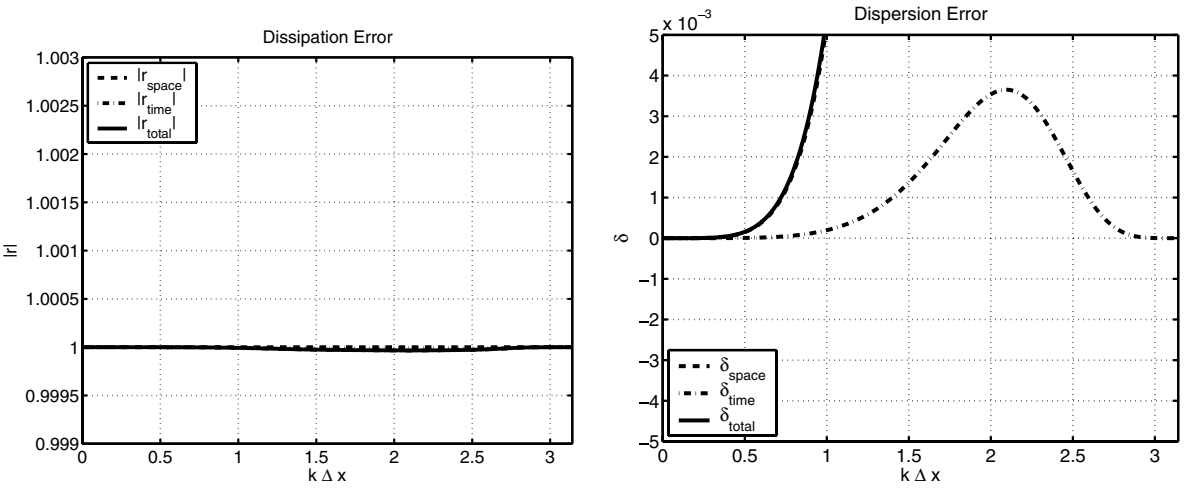

Fig. 5. Dissipation and dispersion errors Calvo optimized RK6, CFL = 0.837.

and Γ specifies the range of exact wave number $k\Delta x$ in the optimization. The difference with the optimization done by other authors is that the time discretization will be optimized locally in the residual footprint and not just for an arbitrary part of the imaginary axis. This allows to optimize the time integration also for upwind type schemes. The integration limit Γ is also more physical because it is the exact wave number range for which the scheme will be optimized.

Since in the optimization process, it is not possible to impose the constraint in Eq. (40) for all $k \in [0,\pi]$, it is only imposed for a discrete amount of wave numbers

$$\begin{aligned} &|G(\mathscr{R}(k_1)\Delta t)| < 1-\epsilon_1, \quad k_1\Delta x \in [0,\pi],\\ &|G(\mathscr{R}(k_2)\Delta t)| < 1-\epsilon_2, \quad k_2\Delta x \in [0,\pi],\\ &\qquad\vdots \end{aligned} \tag{41}$$

A minimum number of constraints is taken to force $|G(-Iak^*\Delta t)| < 1$. ϵ_i is a small number which allows to control the maximum dissipation for wave number k_i. This is necessary sometimes to prevent overshoots of the dissipation error.

3.1. Optimizations for central spatial discretizations

Optimizations for the classical six stage Runge–Kutta scheme given by Eq. (32) have been performed for a fourth order Finite Volume Compact Central (FVCC) spatial discretization [5] at different CFL numbers. The first four coefficients were kept on their default value ($a_n = \frac{1}{n!}$) to keep the scheme fourth order accurate for linear problems (second order accurate for non linear problems). In this optimization process only one constraint was used. Using more constraints with only 2 degrees of freedom (the 5th and 6th coefficient of the Runge–Kutta scheme) leads to imaginary solutions for the coefficients.

In the first optimization, the temporal error was minimized and not the total error. This was done to check whether the optimization process yields similar results as other authors. The following integral was minimized:

$$\int_0^{\Gamma} |G(\mathscr{R}(k\Delta x)\Delta t) - \mathrm{e}^{\mathscr{R}(k\Delta x)\Delta t}|^2 \,\mathrm{d}(k\Delta x). \tag{42}$$

Notice the difference with the integral of Hu et al. in Eq. (36); here the Fourier footprint of the spatial discretization is still plugged in, but the integral minimizes the temporal errors. The constraint was imposed for the wave number $k_1\Delta x = \frac{2\pi}{3}$ which corresponds with the maximum numerical wave number $k_{\mathrm{num}}\Delta x = \sqrt{3}$ of the spatial discretization scheme (see Fig. 6). This wave number corresponds with the highest point of the residual

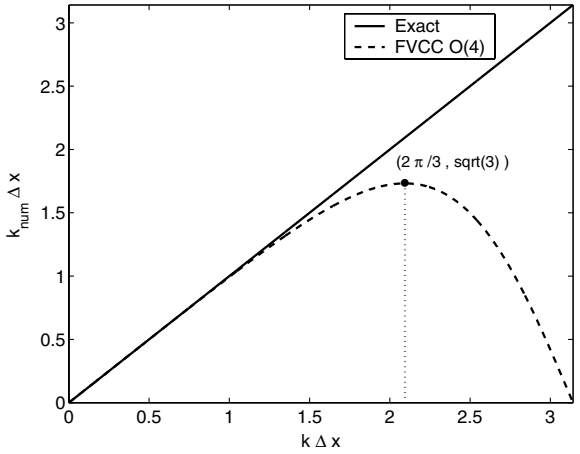

Fig. 6. Resolution of the fourth order FVCC.

footprint on the imaginary axis and therefore the highest total dissipation error. ϵ_1 was tuned until the total dissipation error was smaller than one and Γ was chosen to be equal to $\frac{2\pi}{3}$.

Fig. 7 shows the temporal dissipation and dispersion errors for the optimization for the temporal errors together with those of the schemes proposed by Hu et al. [8] and Calvo et al. [16]. The figure shows that the optimization process gives similar results as the scheme proposed by Hu et al., with a better behavior for the dispersion errors. Comparing the new scheme with the scheme proposed by Calvo et al. [16], it is noted that the latter shows a better behavior for the temporal dissipation errors, but a considerably worse behavior for the dispersion errors.

However when looking at the total errors instead of the temporal errors of the optimized scheme, see Fig. 8, the optimization has an unnoticeable influence on the total dispersion error. This is due to the fact that the dispersion error introduced by the spatial discretization is several magnitudes bigger than that of the temporal discretization error, hence the influence of the optimization can be neglected. For the dissipation error the temporal error equals the total error because the spatial discretization does not introduce any dissipation error. This shows the importance of optimizing for the total error instead of the temporal error.

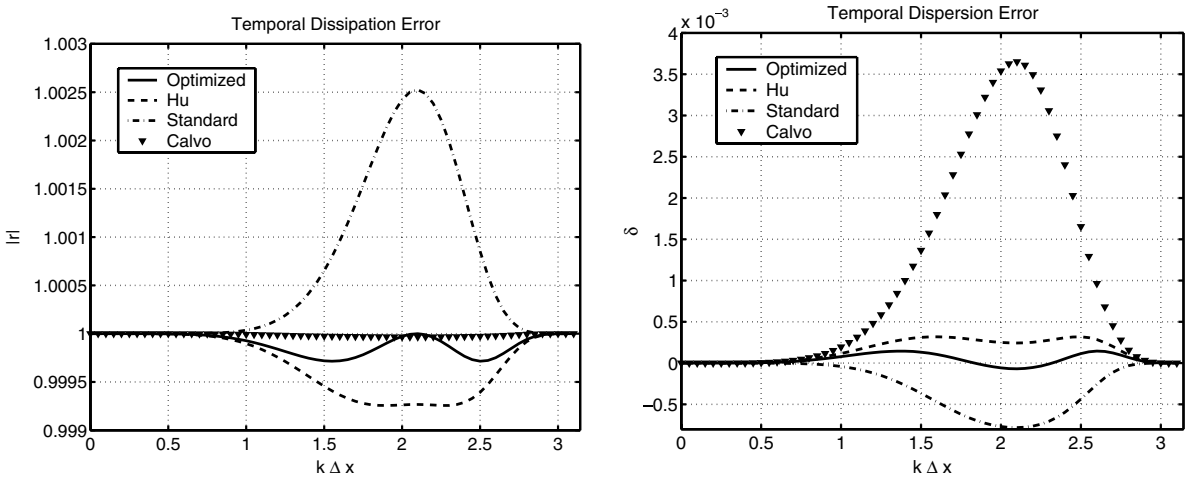

Fig. 7. Temporal dissipation and dispersion errors.

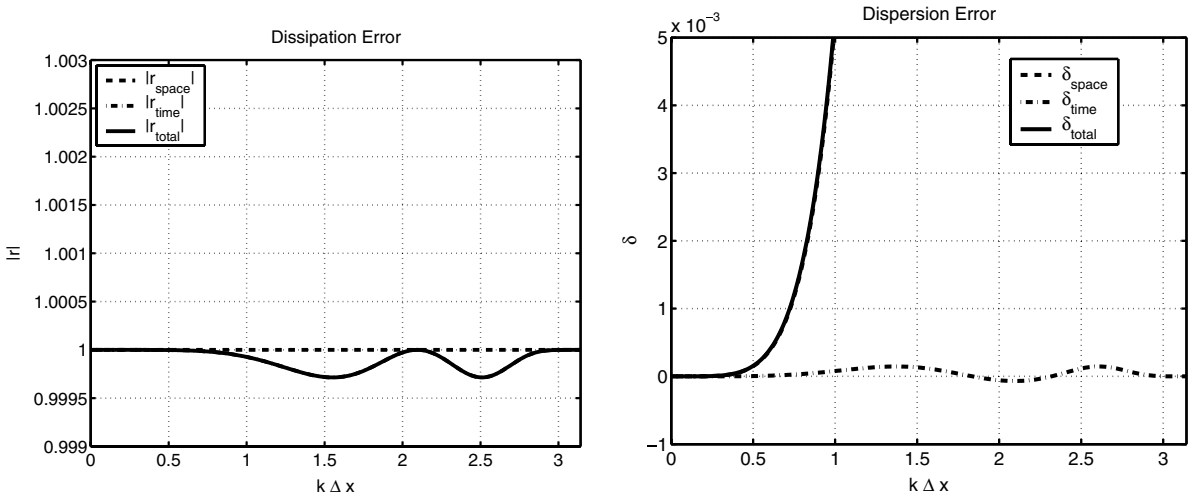

Fig. 8. Total dissipation and dispersion errors.

Thus an optimization was done where the total errors of the six stage Runge–Kutta time integration scheme with fourth order FVCC scheme [5], were minimized with the integral given in Eq. (39). The constraint was imposed for the wave number $k_1\Delta x = \frac{2\pi}{3}$. ϵ_1 was tuned until the total dissipation error was smaller than one and Γ was chosen to be equal to $\frac{2\pi}{3}$. Table 1 gives the optimized coefficients a_5 and a_6 at different CFL numbers.

Beyond a CFL number of 2.1 no more stable schemes could be found. A curve fitting was done on the coefficients. This allows the scheme to be implemented without having to do each time an optimization. Fig. 9 shows the coefficients as a function of the CFL number.

Figs. 10 and 11 shows the temporal resp. total errors for the RK6 scheme optimized for a fourth order FVCC spatial discretization [5] at a CFL of 0.837. The optimization stabilized the scheme which is obvious from the total dissipation error (Fig. 11). When comparing the dispersion error of this optimized scheme (Fig. 12 shows a close-up) to the one of Hu in Fig. 4 or to the one of Calvo et al. in Fig. 5, it is clearly seen that the total dispersion error is better. This is due to the fact that Hu and Calvo only optimized for the temporal error, and did not take into account the spatial error. However, the dissipation error of this optimization is worse than the optimized schemes of Hu and Calvo. The reason is that the optimization tries to compensate

Table 1
Optimized coefficients for six stage RK

CFL	a_5	a_6
0.5	0.156062	0.228422
0.6	0.0611325	0.104581
0.7	0.0255565	0.0528761
0.8	0.0113002	0.0286611
0.9	0.00559034	0.01638
1	0.00352957	0.00979459
1.1	0.0030558	0.00612248
1.2	0.00324681	0.00401757
1.3	0.00367836	0.00278719
1.4	0.00415627	0.00205826
1.5	0.00459567	0.00162286
1.6	0.0049638	0.00136202
1.7	0.00525207	0.00120613
1.8	0.00546249	0.00111362
1.9	0.00560131	0.00105914
2.0	0.00567624	0.00102689
2.1	0.00569541	0.00100682

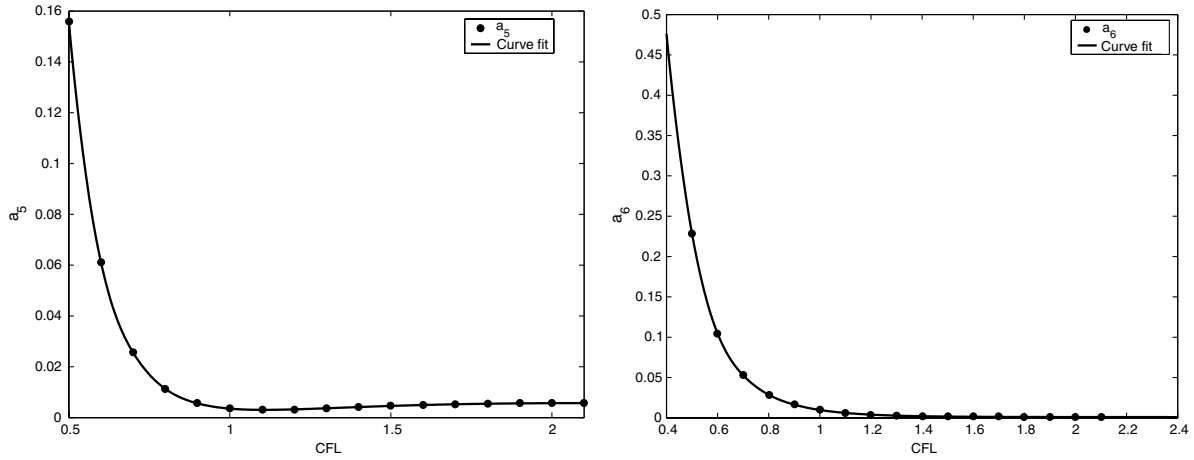

Fig. 9. a_5 and a_6 for the optimized RK6 scheme with compact central spatial discretization.

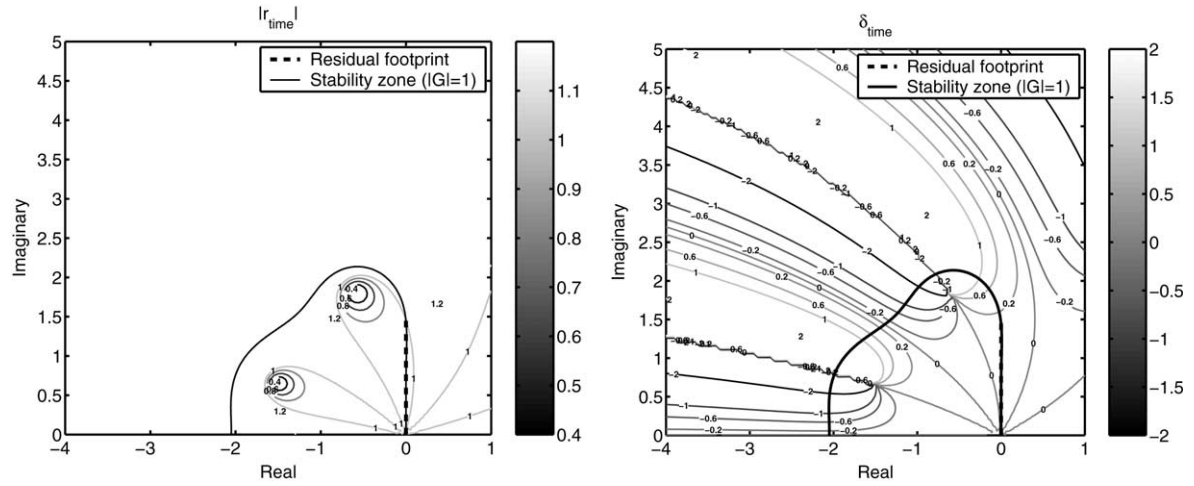

Fig. 10. Temporal dissipation and dispersion error for optimized RK6 with fourth order compact central scheme, CFL = 0.837.

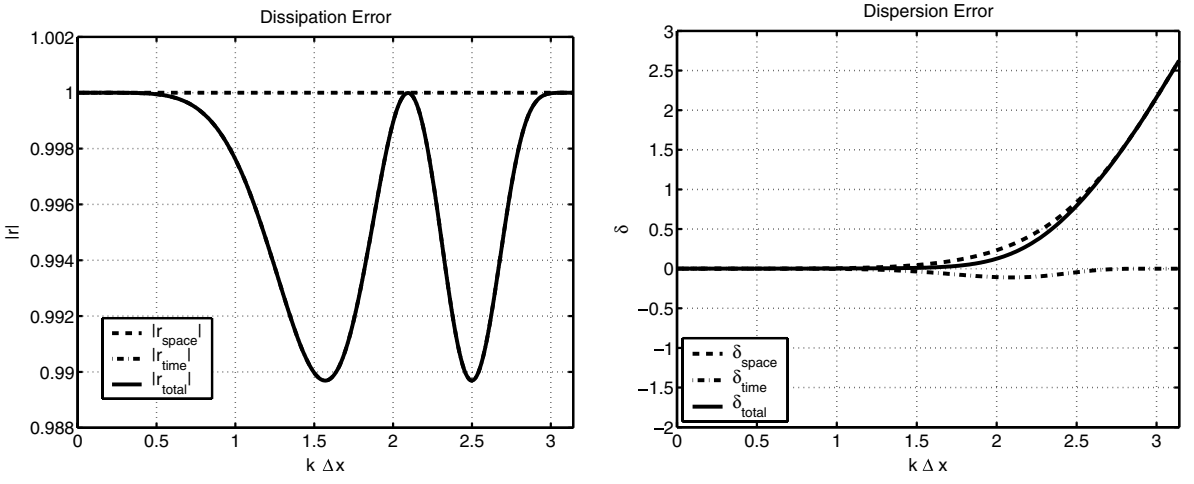

Fig. 11. Total dissipation and dispersion error for optimized RK6 with fourth order compact central scheme, CFL = 0.837.

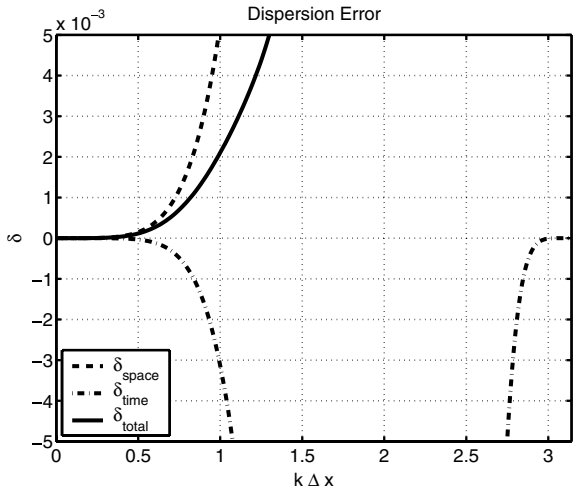

Fig. 12. Zoom of the total dispersion error for optimized RK6 with fourth order compact central scheme, CFL = 0.837.

the large spatial dispersion errors with the temporal dispersion errors to get good total dispersive properties. However, in doing so, the total dissipation errors deteriorate. Still the total error integral given by Eq. (39) is lower for the optimized six stage Runge–Kutta discussed above, than for that of Hu et al. and Calvo et al.

The optimization process will search for the most optimal scheme for a specific CFL number. Therefore stable schemes for higher CFL numbers can be found. In realistic CAA applications however, waves will travel at different speeds and therefore locally the CFL number can be lower then the maximum CFL number for which the scheme was optimized. Fig. 13 shows the six stage Runge–Kutta scheme optimized for a CFL number of 1.2. On the left figure the total dissipation errors are shown and it is noted that for lower CFL numbers the dissipation errors converge monotonically towards one. The right figure shows the total and the spatial errors for the optimized Runge–Kutta scheme. For smaller CFL numbers the total dispersion error converge towards the spatial dispersion error. This is due to the fact that for smaller CFL numbers the temporal errors converges faster to zero then the spatial errors and thus the spatial errors will be the dominant term in the total dispersion errors. This will be true for any Runge–Kutta scheme, whether optimized or not.

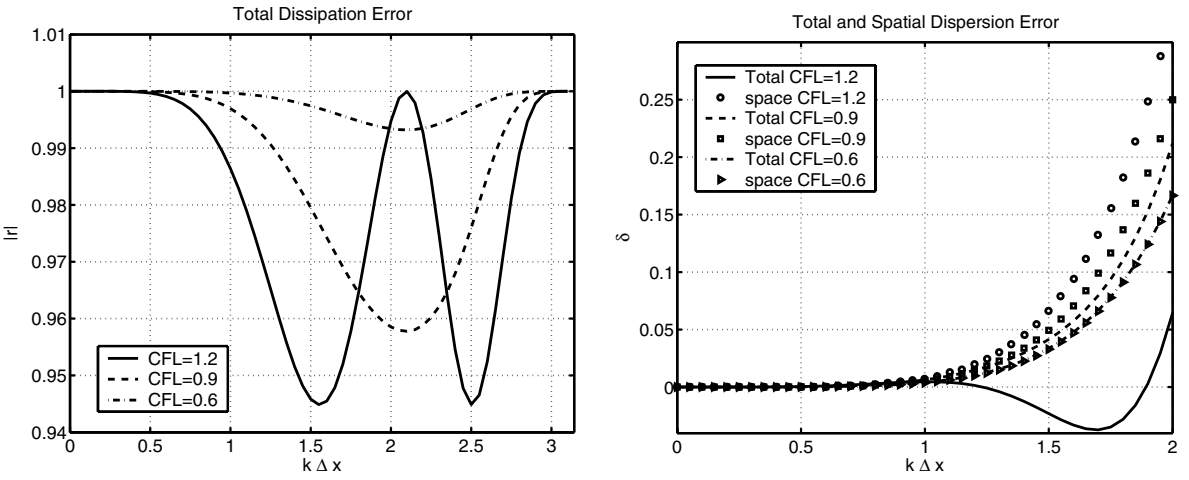

Fig. 13. Dissipation and dispersion error for RK6 optimized for CFL = 1.2 with fourth order compact central scheme.

3.2. Optimizations for upwind spatial discretizations

Using the same strategy as for the central spatial discretizations, optimizations for a six stage Runge–Kutta scheme, given by Eq. (35), were performed for a 3rd order Finite Volume Upwind scheme (43).

$$u_{i+\frac{1}{2}} = -\frac{u_{i-1}}{6} + \frac{5u_i}{6} + \frac{u_{i+1}}{3}. \tag{43}$$

In a first attempt, the same approach as for the central schemes was used. The first four coefficients were kept on their default value, while the last two were left free for the optimization process. One constraint was used to keep the total dissipation error lower than one. The wave number where the constraint was imposed, was chosen arbitrarily because for upwind schemes it is not clear at which wave number the maximum dissipation error occurs (cf. central schemes). Table 2 gives the optimized coefficients a_5 and a_6 for the optimized six stage Runge–Kutta time integration at different CFL numbers.

Figs. 14 and 15 show the temporal resp. total errors for the RK6 scheme optimized for a 3rd order Finite Volume Upwind spatial discretization at a CFL of 1.

Fig. 15 shows that the total dispersion error is negative for the lower wave number. This means the waves in that wave number range will run ahead and thus one will have both trailing and leading error waves.

To prevent this, a second optimization was done. In this optimization a third coefficient of the six stage Runge–Kutta time integration was left free so that an extra constraint, keeping the total dispersion error positive, could be imposed. This was done using Eq. (44):

$$\begin{aligned} &|G(\mathscr{R}(k_1\Delta x)\Delta t)| < 1 - \epsilon_1, \quad k_1\Delta x \in [0,\pi], \\ &\delta(\mathscr{R}(k_2\Delta x)\Delta t) > \epsilon_2, \quad k_2\Delta x \in [0,\pi]. \end{aligned} \tag{44}$$

Table 2
Coefficients for RK6,with 3rd order upwind spatial discretization and 1 constraint

CFL	a_5	a_6
0.5	0.233527741907065	−1.811438359723931
1	0.060972922581029	−0.029022426455235
1.5	0.021010664194455	0.001785523026951
2	0.010501303982894	0.002144008620393

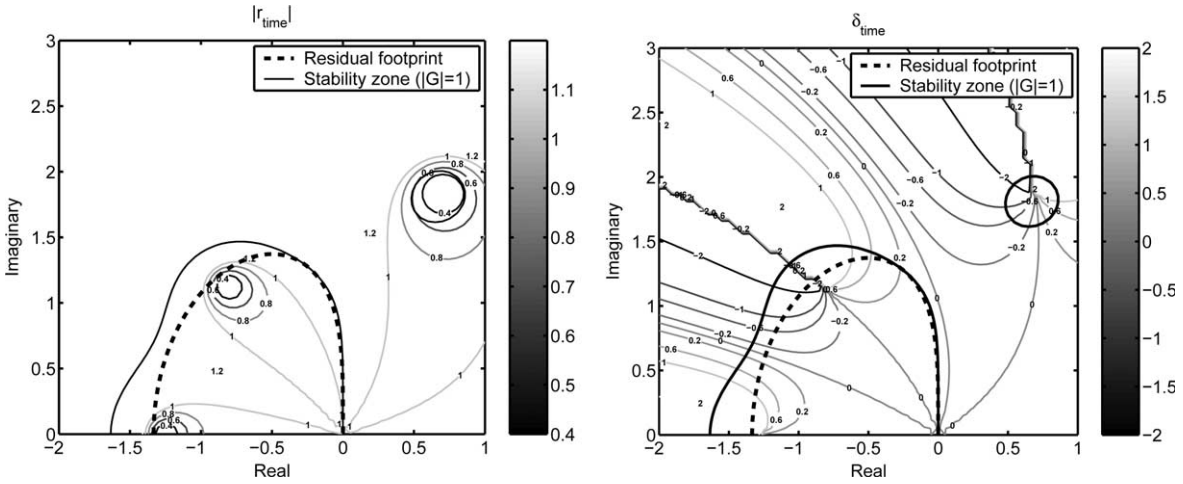

Fig. 14. Temporal dissipation and dispersion error for optimized RK6 with a 3rd order upwind scheme, CFL = 1.

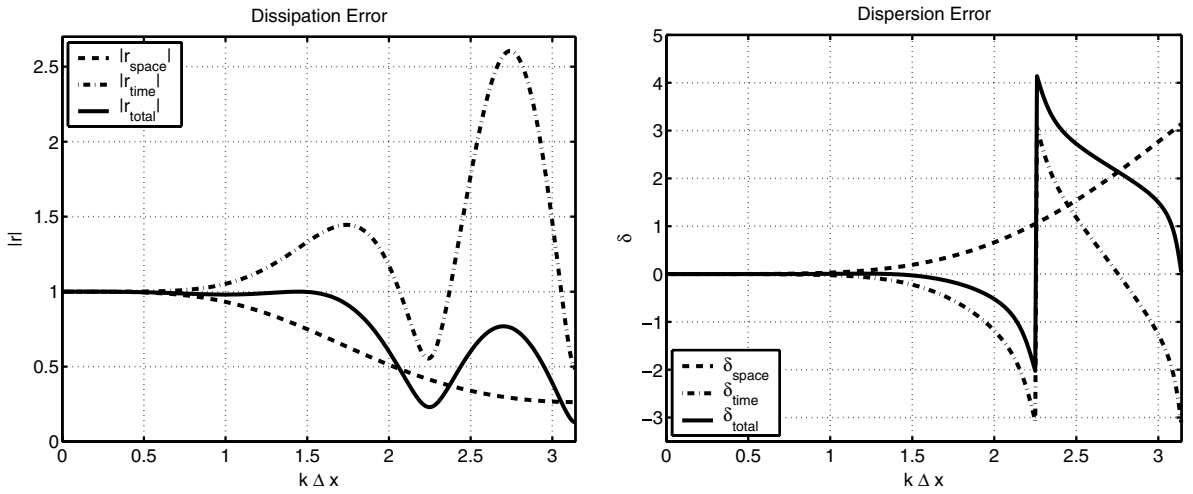

Fig. 15. Total dissipation and dispersion error for optimized RK6 with 3rd order upwind scheme, CFL = 1.

Here ϵ_2 is an arbitrary small positive number, tuned so that the total dispersion error is positive. For the optimization the parameters where chosen as follow: $\Gamma = 0.7$ and $\epsilon_2 = 0.001$. The other parameters (k_1, ϵ_1, k_2) were tuned to get a stable scheme. The optimization was done for several CFL numbers given in Table 3.

Figs. 16 and 17 show the temporal resp. total errors for the RK6 scheme optimized with 2 constraints, one to keep the dissipation error lower than 1 and the other to keep the dispersion error positive, at a CFL of 1.

Fig. 17 shows that the total dispersion error is positive for all the wave numbers with this optimization process.

4. Results

4.1. 1D convection equation

4.1.1. Central spatial discretizations

To confirm the results of the previous sections and check the behavior of dissipation and dispersion error, Eq. (1) is solved for a one-dimensional disturbance propagated over a long distance. For the discretization the fourth order Finite Volume Compact Central (FVCC) spatial discretization [5] was used together with the optimized time integration scheme. The initial disturbance at $t = 0$ is given by:

Table 3
Coefficients for RK6,with 3rd order upwind spatial discretization and 2 constraints

CFL	a_4	a_5	a_6
0.5	0.6103585735342473	0.7275827775574703	1.011484539315444
0.6	0.3752938322936234	0.3819408030144663	0.3900640950322403
0.7	0.2447703272913577	0.2237926707106628	0.1293917897285167
0.8	0.1805088055415769	0.1443231536384547	0.07799879077996832
0.9	0.1298698302104733	0.09592895796572629	0.03311940330994816
1	0.1067896454477023	0.06931071638970879	0.02214886830986389
1.1	0.09153849890351894	0.05218741811771738	0.01652759824747786
1.2	0.081584	0.0411344	0.0120665
1.3	0.07213944773744652	0.03262501366485934	0.008502824530748406
1.4	0.06792744758580115	0.02723553471697291	0.008424947675876551
1.5	0.06243260779861243	0.0225065918724392	0.006160913210227391

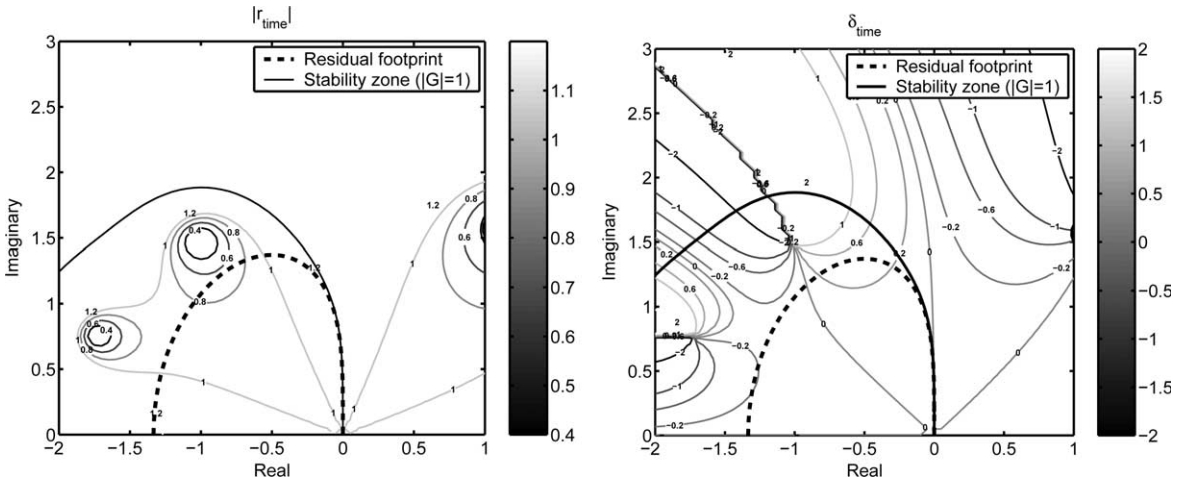

Fig. 16. Temporal dissipation and dispersion error for optimized RK6 with 2 constraints, CFL = 1.

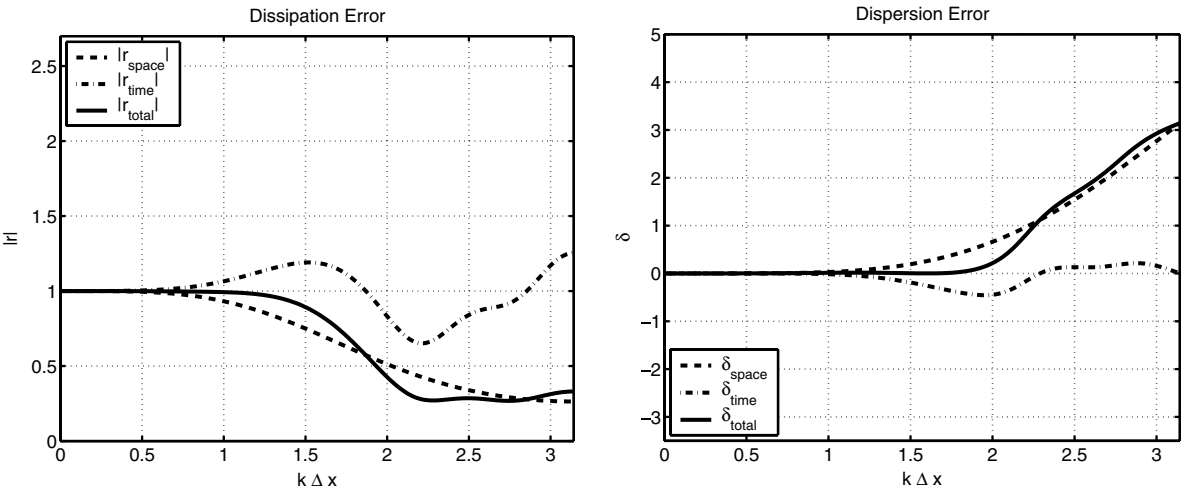

Fig. 17. Total dissipation and dispersion error for optimized RK6 with 2 constraints, CFL = 1.

$$u(x) = \sin\left(\frac{2\pi x}{a\Delta x}\right)\exp\left(-\ln(2)\left(\frac{x}{b\Delta x}\right)^2\right), \tag{45}$$

where $a = 16$, $b = 3$, $\Delta x = 1$ and the propagation speed is 1. The disturbance was propagated over a distance of $300\Delta x$. Fig. 18 shows the result for a CFL number of 0.837, which corresponds to the accuracy limit of the scheme of Hu. The left figure shows the results with the optimized Runge–Kutta scheme proposed by Hu, while on the right figure the results are shown for the present, total error optimized Runge–Kutta scheme. Looking at the trailing oscillations it is clear that the dispersive properties of the latter scheme are better, as predicted in previous section. Fig. 19 shows the error given by $|u - u_{\text{initial}}|$ of both calculations. It is clearly seen that the optimization for the total error yields better results.

The test case above was also calculated at a CFL number 1.2 to compare the optimized RK6 scheme with the one of Calvo et al [16]. Fig. 20 shows the signal after it was propagated over a distance $300\Delta x$. The left figure shows the results for the scheme of Calvo, while the right figure shows the result for the total error optimized scheme. Also here the latter scheme shows less trailing oscillations. Fig. 21 shows the error given by

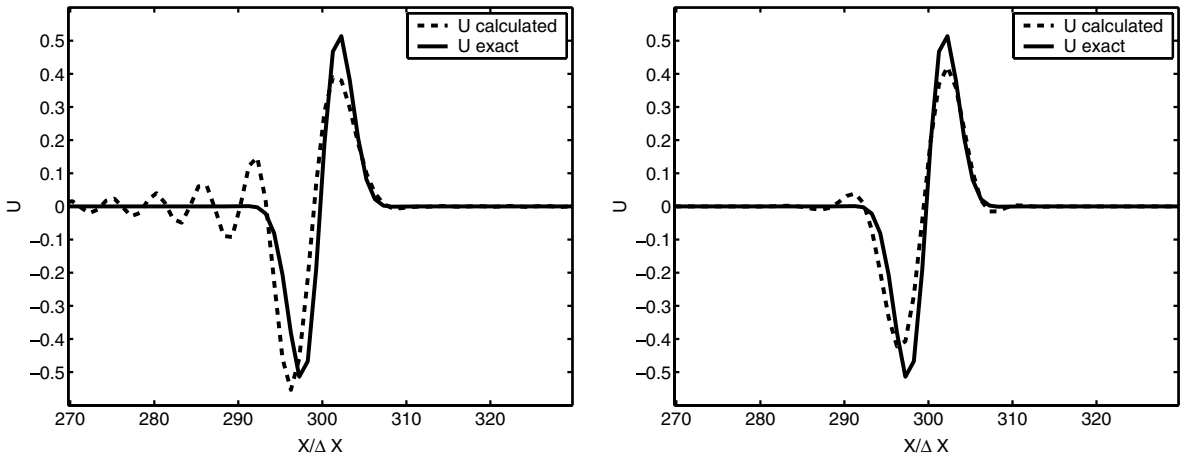

Fig. 18. Optimization of Hu (left) Own optimization (right); CFL = 0.837 (central).

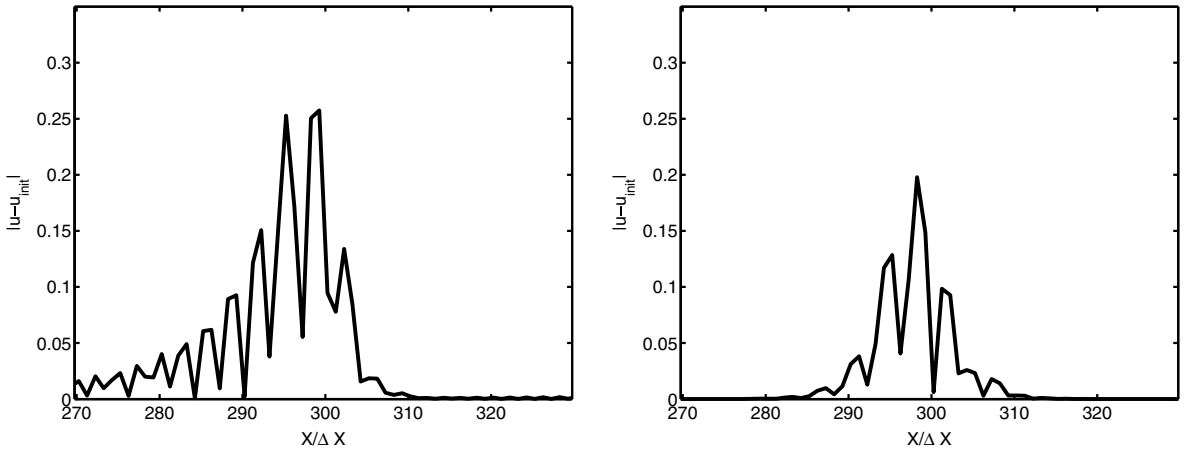

Fig. 19. Optimization of Hu (left) Own optimization (right); CFL = 0.837 (central).

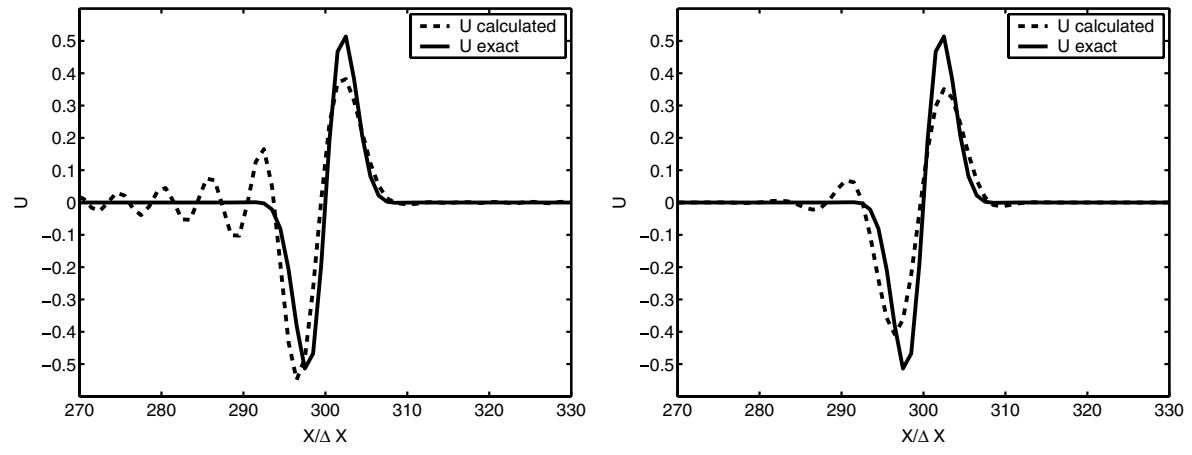

Fig. 20. Optimization of Calvo (left) Own optimization (right); CFL = 1.2 (central).

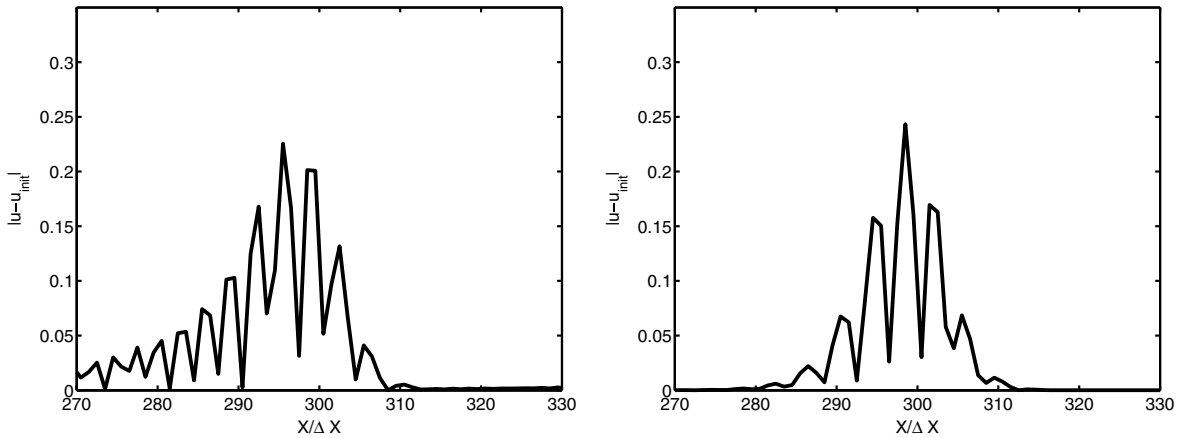

Fig. 21. Optimization of Calvo (left) Own optimization (right); CFL = 1.2 (central).

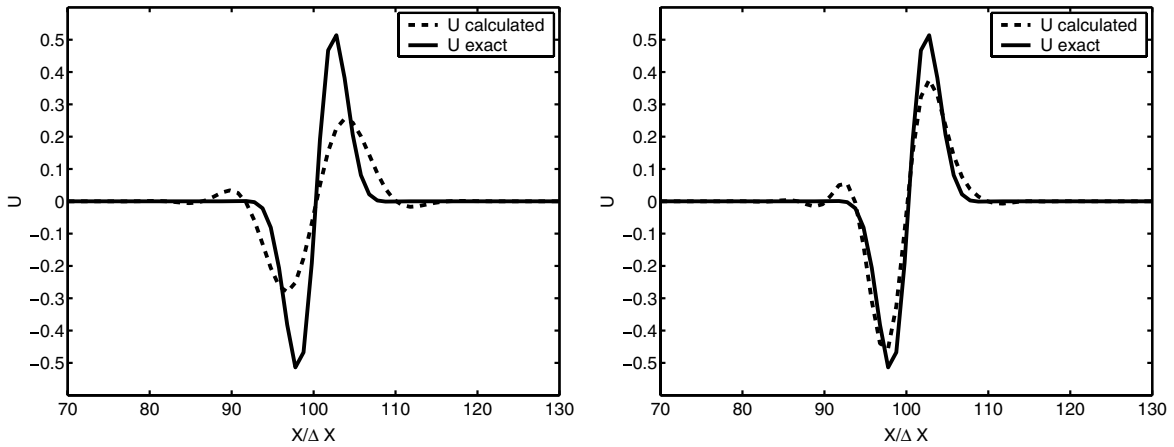

Fig. 22. Standard RK6 (left); Optimized RK6 (right); CFL = 0.97358 (upwind).

$|u - u_{\text{initial}}|$ of both calculations. Comparing the amplitudes of the error it is noticed that the scheme of Calvo shows less dissipation than the scheme by Hu et al. (even though this calculation was run at a higher CFL). The total error optimized scheme shows a similar amount of dissipation than the scheme by Calvo. However the former scheme has a less spread out error, indicating a better dispersive behavior.

4.1.2. Upwind spatial discretizations

To test the optimized Runge–Kutta schemes for an Upwind spatial discretization the same test case as in Section 4.1.1 was done. Fig. 22 shows the result for a CFL number of 0.97358, this is the CFL number given by the accuracy limit of Hu et al. (to be able to compare with his scheme). The left figure shows the standard six stage Runge–Kutta scheme while the right figure shows the optimized scheme.

Fig. 23 shows the error given by $|u - u_{\text{initial}}|$ of both calculations. The error is more or less reduced by 50 percent in amplitude.

For comparison the test case was rerun with the optimized scheme of Hu et al. at the same CFL, Fig. 24. It is observed that almost no improvement is obtained as compared to the standard six stage Runge–Kutta scheme. This is not surprising as the Hu scheme only optimizes along the imaginary axis without accounting for the spatial scheme, which, in this case, has its footprint in the full complex plane.

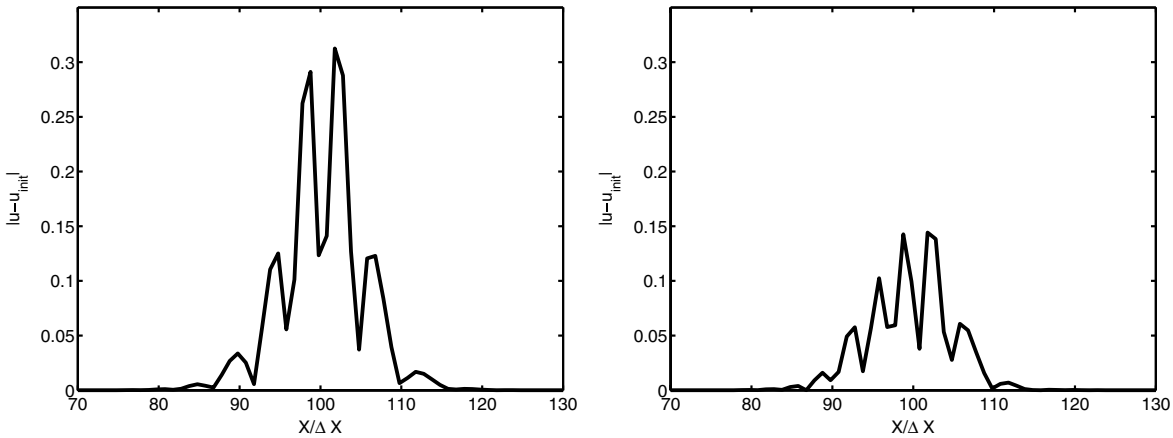

Fig. 23. Standard RK6 (left); Optimized RK6 (right); CFL = 0.97358 (upwind).

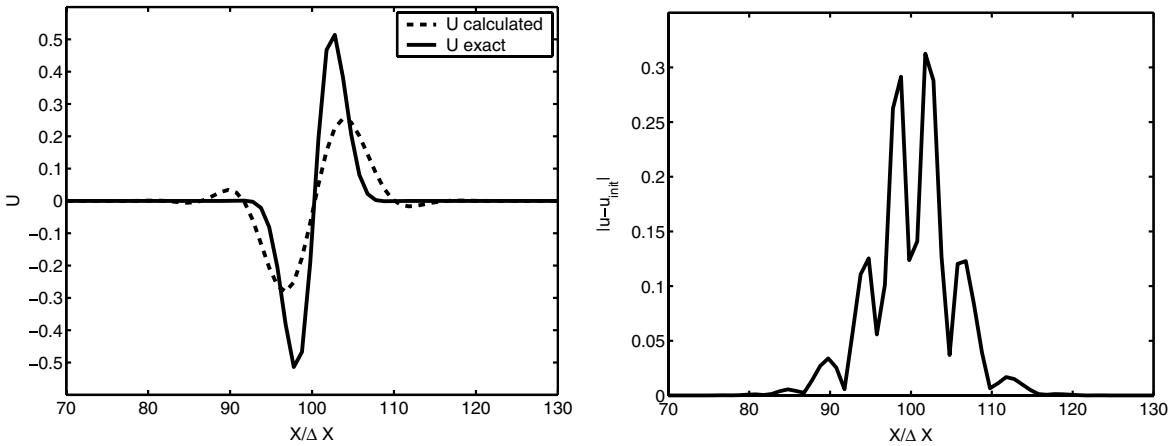

Fig. 24. Optimized Hu RK6 (left); Optimized Hu RK6 error (right); CFL = 0.97358 (upwind).

4.2. Linearized Euler equations

To test the performance of the optimizations for CAA applications the one dimensional Linearized Euler Equations (LEE) given by Eq. (46) were solved.

$$\frac{\partial U}{\partial t} + A\frac{\partial U}{\partial x} = 0, \tag{46}$$

where U, the vector of primitive variables, and A are given by:

$$U = \begin{pmatrix} \rho \\ u \\ p \end{pmatrix}, \quad A = \begin{pmatrix} u_0 & \rho_0 & 0 \\ 0 & u_0 & \frac{1}{\rho_0} \\ 0 & \gamma p_0 & u_0 \end{pmatrix}. \tag{47}$$

Eq. (46) can be written under diagonal form:

$$\frac{\partial W}{\partial t} + B\frac{\partial W}{\partial x} = 0, \tag{48}$$

where W, the vector of characteristic variables, and B are given by:

$$W = \begin{pmatrix} \frac{1}{2}\left(\frac{p}{\rho_0 c} - u\right) \\ \rho - \frac{p}{c^2} \\ \frac{1}{2}\left(\frac{p}{\rho_0 c} - u\right) \end{pmatrix}, \quad B = \begin{pmatrix} u_0 - c & 0 & 0 \\ 0 & u_0 & 0 \\ 0 & 0 & u_0 + c \end{pmatrix} \tag{49}$$

and $c = \sqrt{\gamma \frac{p_0}{\rho_0}}$ is the speed of sound. In case of a subsonic regime, $0 < u_0 < c$, the acoustic wave w_1 will travel upstream and w_3 downstream with speeds resp. equal to $u_0 - c$ and $u_0 + c$. The entropy wave w_2 travels downstream with a speed equal to u_0.

The calculation was done using the fourth order FVCC schemes described in [5] together with the optimized six stage Runge–Kutta schemes. On the boundaries periodicity was imposed. The domain with length $L = 100$ was divided into cells of width $\Delta x = 0.025$. The CFL number was chosen to be CFL $= 0.83732$. The time step was calculated from the CFL number:

$$\Delta t = \mathrm{CFL}\frac{\Delta x}{u_0 + c} \tag{50}$$

resulting in $\Delta t = 0.01608$. The speed was chosen to be $u_0 = \frac{c}{10}$. The other parameters were set to: $\gamma = 1.4$, $p_0 = 1$ and $\rho_0 = 1$. The initial conditions were:

$$\begin{cases} \rho(x,0) &= \mathrm{e}^{-250(x-50)^2}, \\ u(x,0) &= 2\mathrm{e}^{-250(x-50)^2}, \\ p(x,0) &= 0. \end{cases} \tag{51}$$

This initial flow field is a superposition of two gaussian acoustic waves (left and right travelling) and a gaussian entropy wave. All results shown below are obtained after 1000 time steps or $t = 16.08$.

Fig. 25 shows the density, while Fig. 26 shows the error on the density. Important oscillations can be observed behind the waves. This is due to the rather big dispersion error of the standard RK6 scheme (given in Fig. 3). It is clear that the errors are the lowest for the entropy wave and the highest for the right travelling acoustic wave. This is due to the fact that the entropy wave travels at a speed u_0 while the right travelling acoustic wave travels at a speed of $u_0 + c$. This means that locally the CFL number for the entropy wave is a lot smaller resulting in smaller errors.

The results of the optimized schemes are shown in Fig. 27. One notices immediately the lower trailing oscillations behind the acoustic waves. The trailing waves behind the entropy wave are of the same order as those of the standard RK6 scheme.

The errors of the acoustic waves for the optimized RK6 scheme, shown in Fig. 28, are smaller in amplitude and less spread out in space, compared to those of the standard RK6 scheme (shown in Fig. 26). The errors for the entropy wave are of the same order of magnitude as those of the standard RK6 scheme. As mentioned above, the left and right travelling acoustic waves are travelling at speeds of resp. $u_0 - c$ and $u_0 + c$, while the entropy wave travels at a speed of u_0. Since the optimizations are done for a certain CFL number, based on the speed $u_0 + c$, the optimizations will be most effective for waves travelling at speeds around $u_0 + c$. For low speed flows where $u_0 \ll c$, and thus $|u0 + c| \approx |u_0 - c| \approx c$ the optimizations will show significant improvement for all acoustic waves. The optimization will be less efficient on the entropy waves. However since here the CFL number is so small, and thus so are the errors, the need for minimizing the errors is less stringent.

Figs. 29 and 30 show resp. the density and the error on the density for the optimized RK6 scheme by Hu et al. [8]. The scheme still shows lots of trailing waves due to its total dispersion error (see Fig. 4). There is only little difference with the standard RK6 scheme because although the temporal dispersion error was minimized, the optimization had little effect on the total dispersion error (see Fig. 4).

The same calculation was done at a higher CFL number of 1.2. The results shown below are after 800 time steps or at time $t = 18.43973$. They are compared with the optimized scheme by Calvo et al. [16]. Figs. 31 and 32 show resp. the density and the error on the density for the total error optimized RK6. Comparing these results with the ones obtained with Calvo's optimized scheme in Figs. 33 and 34, same conclusions as before can be drawn: the total error optimized scheme shows a better dispersive behavior then the scheme proposed

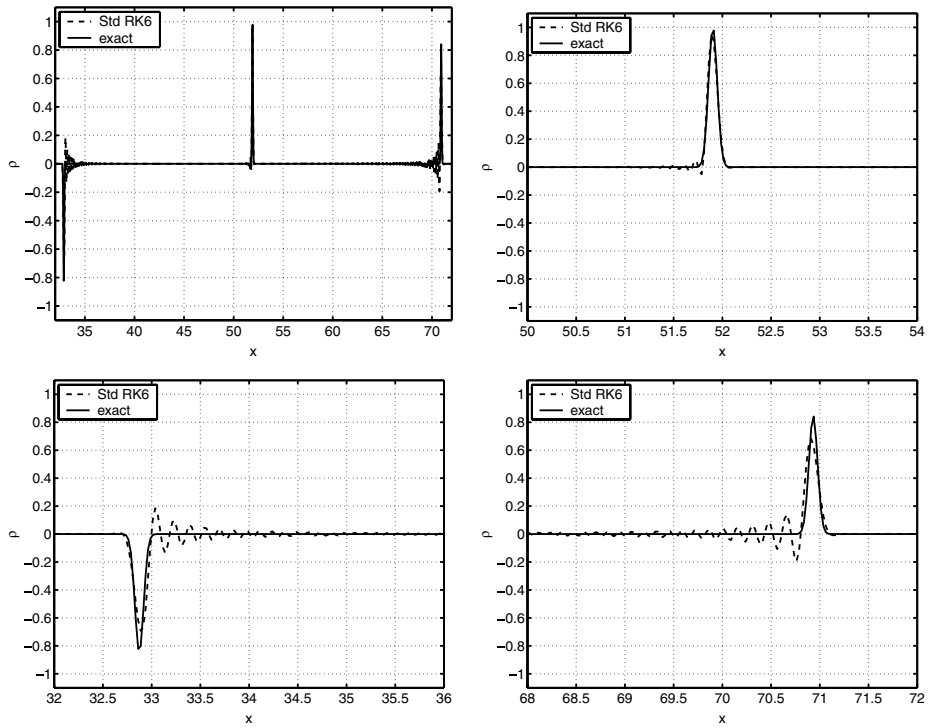

Fig. 25. Density plot for standard RK6: whole field (top left); entropy wave (top right); left acoustic wave (bottom left); right acoustic wave (bottom right).

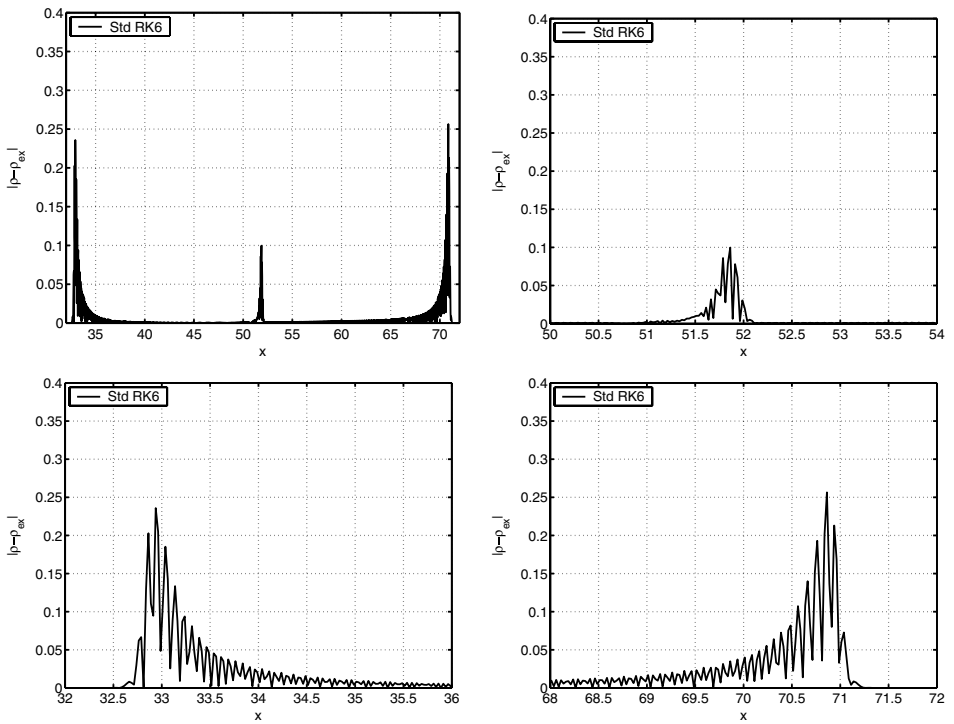

Fig. 26. Density error plot for standard RK6: whole field (top left); entropy wave (top right); left acoustic wave (bottom left); right acoustic wave (bottom right).

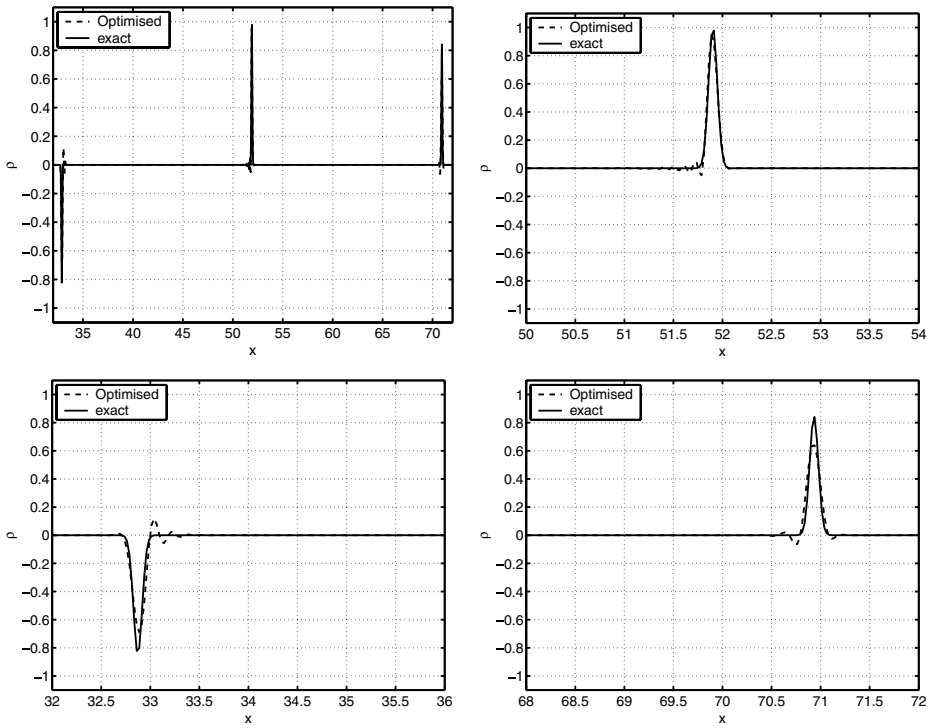

Fig. 27. Density plot for optimized RK6: whole field (top left); entropy wave (top right); left acoustic wave (bottom left); right acoustic wave (bottom right).

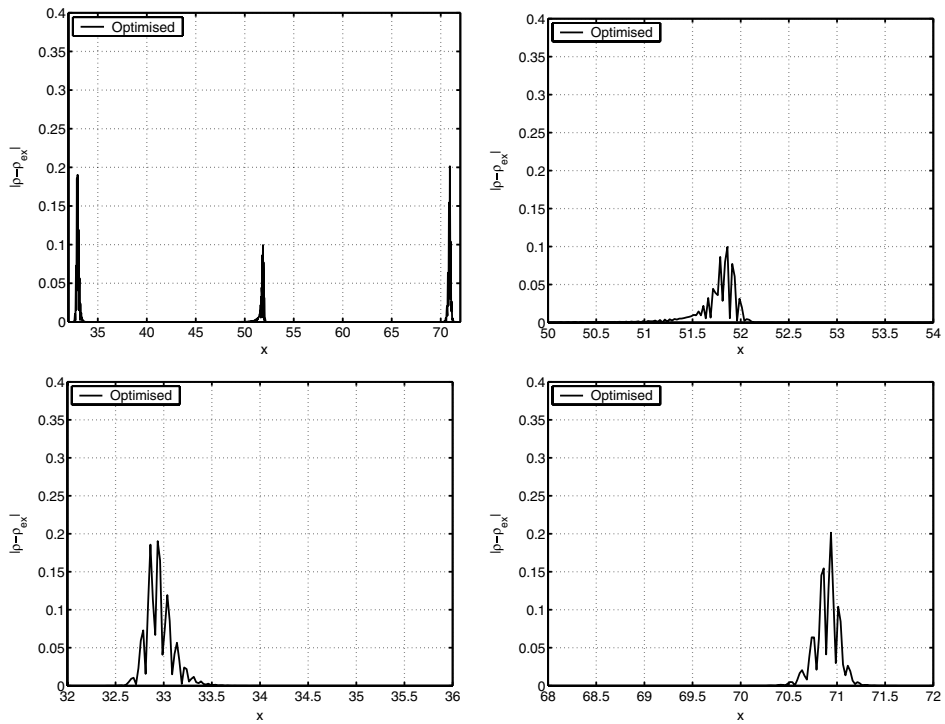

Fig. 28. Density error plot for optimized RK6: whole field (top left); entropy wave (top right); left acoustic wave (bottom left); right acoustic wave (bottom right).

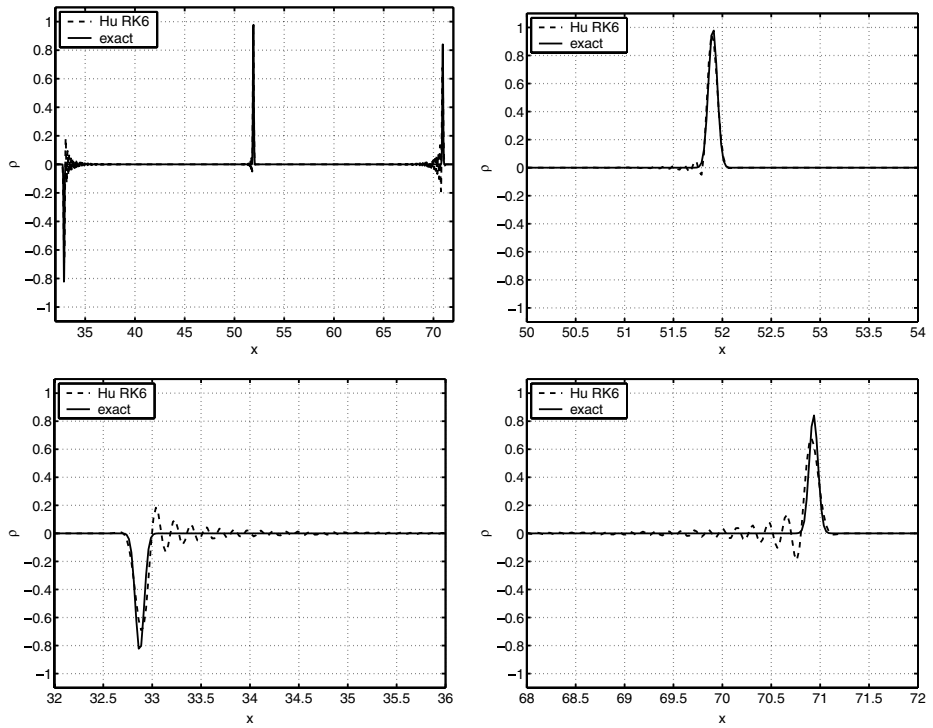

Fig. 29. Density plot for RK6 of Hu et al., whole field (top left); entropy wave (top right); left acoustic wave (bottom left); right acoustic wave (bottom right).

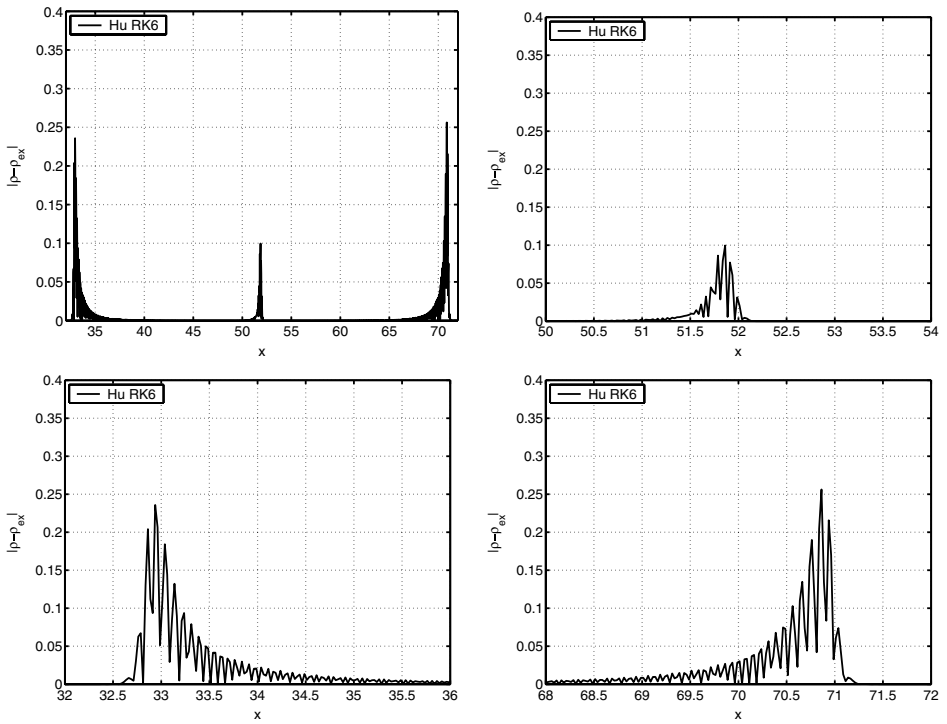

Fig. 30. Density error plot for RK6 of Hu et al., whole field (top left); entropy wave (top right); left acoustic wave (bottom left); right acoustic wave (bottom right).

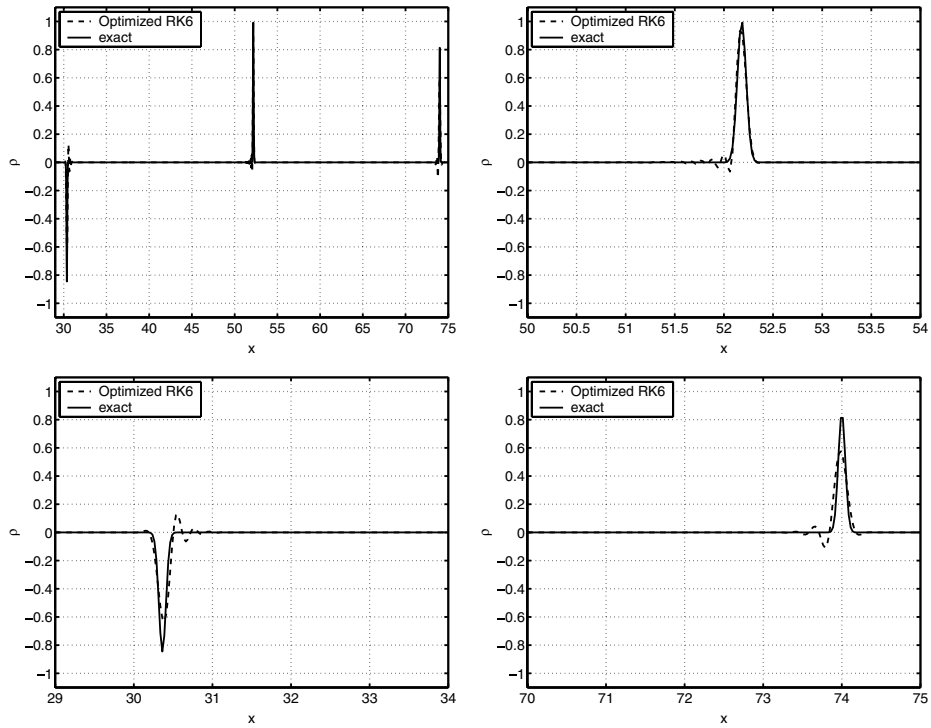

Fig. 31. Density plot for optimized RK6 CFL = 1.2: whole field (top left); entropy wave (top right); left acoustic wave (bottom left); right acoustic wave (bottom right).

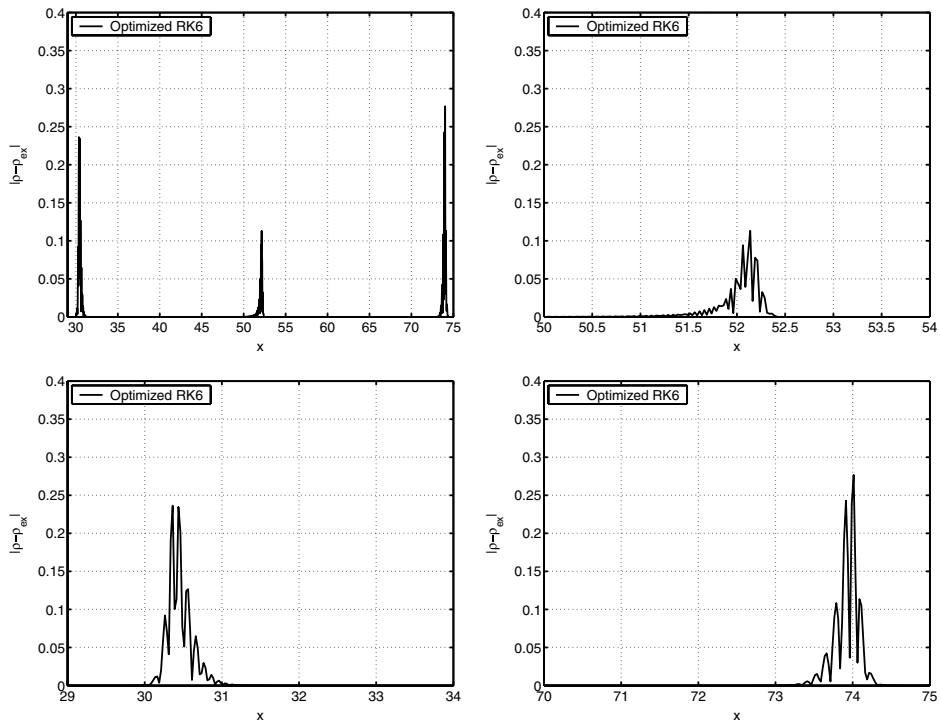

Fig. 32. Density error plot for optimized RK6 CFL = 1.2: whole field (top left); entropy wave (top right); left acoustic wave (bottom left); right acoustic wave (bottom right).

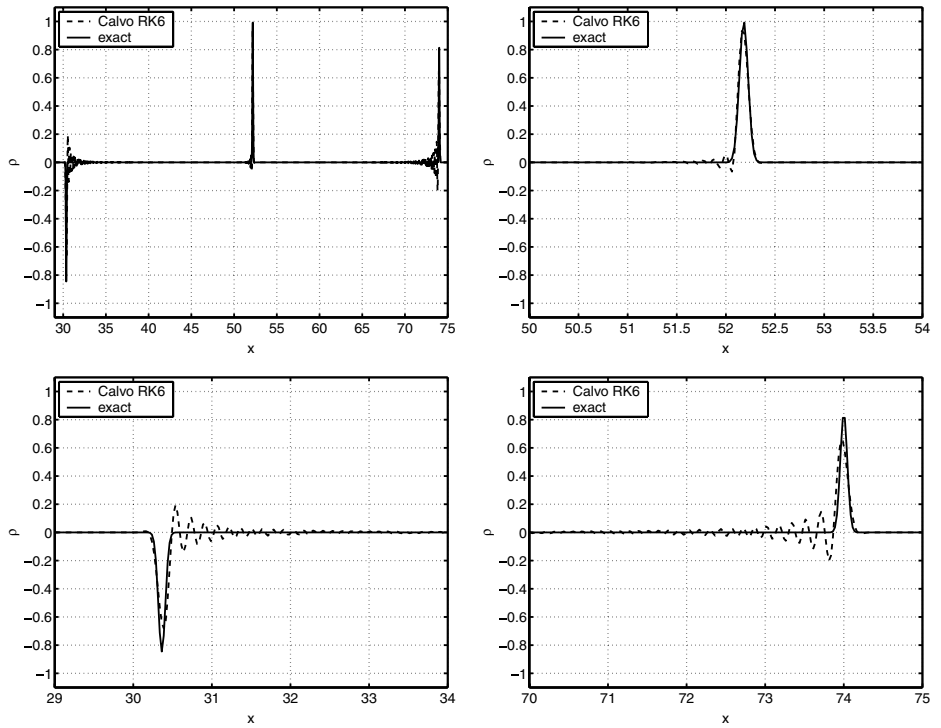

Fig. 33. Density plot for RK6 of Calvo et al. CFL = 1.2: whole field (top left); entropy wave (top right); left acoustic wave (bottom left); right acoustic wave (bottom right).

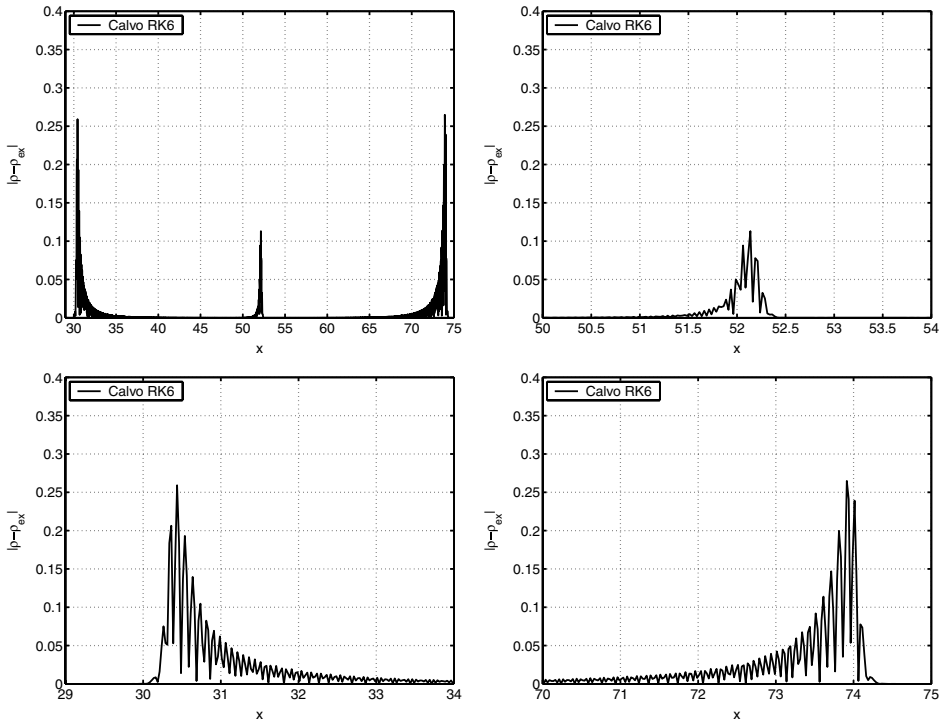

Fig. 34. Density error plot for RK6 of Calvo et al. CFL = 1.2: whole field (top left); entropy wave (top right); left acoustic wave (bottom left); right acoustic wave (bottom right).

by Calvo. The error is less spread in space and the amplitudes are of similar order, showing again the efficiency of optimizing for the total errors instead of the temporal errors.

5. Conclusions

In this article the errors arising from spatial and temporal discretization were discussed. A new way of optimizing time integration schemes has been formulated. The proposed approach allows to optimize time integration schemes, taking also the spatial discretization into account. This leads to a minimization of the total dissipation and dispersion errors. Optimizations were done on a six stage explicit Runge–Kutta scheme in combination with a fourth order Finite Volume Central Compact scheme and a 3rd order Finite Volume Upwind scheme. The optimizations were compared with the optimizations of Hu et al. [8] and Calvo et al. [16] and found to show better properties. Calculations were done for a 1D convection of a wave at a low and a higher CFL number. The results confirmed the improvements of the optimizations and also showed that one should be careful when using classical optimized temporal schemes in combination with dissipative spatial discretizations. The improved accuracy using the present methodology was also confirmed in a Linearized Euler test case.

References

[1] N.A. Adams, K. Shariff, A high-resolution hybrid compact-ENO scheme for shock-turbulence interaction problems, Journal of Computational Physics 127 (1996) 27–51.
[2] S.K. Lele, Compact finite difference schemes with spectral-like resolution, Journal of Computational Physics 103 (1992) 16–42.
[3] J.W. Kim, D.J. Lee, Optimized compact finite difference schemes with maximum resolution, AIAA Journal 34 (1996) 5.
[4] Chris Lacor, Sergey Smirnov, Martine Baelmans, A finite volume formulation of compact central schemes on arbitrary structured grids, Journal of Computational Physics 198 (2004) 535–566.
[5] Broeckhoven Tim, Smirnov Sergey, Ramboer Jan, Lacor Chris, Finite volume formulation of compact upwind and central schemes with artificial selective damping, SIAM Journal of Scientific Computing 21 (3) (2004) 341–367.
[6] J.M.C. Pereira, M.H. Kobayashi, J.C.F. Pereira, A fourth-order-accurate finite volume compact method for the incompressible Navier–Stokes solutions, Journal of Computational Physics 167 (2001) 217–243.
[7] C.A. Kennedy, M.H. Carpenter, R.M. Lewis, Low-Storage Explicit Runge–Kutta Schemes for the Compressible Navier–Stokes Equations, ICASE Report No. 99-22, 1999.
[8] F.Q. Hu, M.Y. Hussani, J.L. Manthey, Low-dissipation and low-dispersion Runge–Kutta schemes for computational acoustics, Journal of Computational Physics 124 (1996) 177–191.
[9] J.W. Goodrich, A comparison of numerical methods for computational aeroacoustics, AIAA paper 99-1943, 1999.
[10] C.K.W. Tam, J.C. Webb, Dispersion-relation-preserving finite difference schemes for computational acoustics, Journal of Computational Physics 107 (1993) 262–281.
[11] R. Ewert, M. Meinke, W. Schröder, Comparison of source term formulations for a hybrid CFD/CAA method, AIAA paper 2001-2200, 2001.
[12] C. Bogey, C. Bailly, D. Juvé, Computation of mixing layer noise using large eddy simulation, AIAA paper 99-1871, 1999.
[13] C. Bogey, C. Bailly, D. Juvé, Numerical simulation of sound generated by Vortex pairing in a mixing layer, AIAA Journal 38 (2000) 2210–2218.
[14] P.J. Morris, L.N. Long, A. Bangalore, Q. Wang, A parallel three-dimensional aeroacoustics method using nonlinear disturbance equations, Journal of Computational Physics 133 (1997).
[15] C. Bogey, C. Bailly, A family of low dispersive and low dissipative explicit schemes for flow and noise computations, Journal of Computational Physics 194 (2004) 194–214.
[16] M. Calvo, J.M. Franco, L. Rández, A new minimum storage Runge–Kutta scheme for computational acoustics, Journal of Computational Physics 201 (2004) 1–12.